CHAPTER 3

RESULTS

CHAPTER 3

RESULTS

3.1 The Structure of lead smelter industry in Egypt.

Table (7) shows the structure of lead smelters in Egypt. It is seen that 30 rotary furnaces, 18 kettle furnaces and 7 shaping machines are installed and currently working in 14 plants. Only one plant is a public sector (GEMET) locating at El-Tebbin; South Cairo, while all the other lead smelters are private sector. Most of lead smelter plants are located in Great Cairo and Alexandria.

3. 2 Types of lead smelting furnaces.

Two types of furnaces are available; lead smelter for recovery of lead from scrap batteries and kettle furnace for refining of hard lead. The first operates at high temperature level (> 1450 °C) while the second operates at low temperatures (< 650°C).

3.2.1 Specific variants of the rotary furnaces.

According to direct visits and precise classification, specific variants of lead smelters can be categorized into two main types; very short (about 3 m long and 1.75 m in diameter) and short rotary furnaces (5.25 m long and 2.4 m in diameter). In some cases lead plants are furnished with only one smelter, others may operate 3 lead furnaces.

A survey of baseline study of lead smelters (devoted only to the private sector) in Egypt was carried out by the Technical Cooperation Office for the Environment (TCOE) of the Egyptian Environmental Affairs Agency (EEAA) to quantify lead production. The data so issued was further updated whereby other plants were inserted.

Table (7) The Structure of lead smelter industry in Egypt.

Owner	location	furnace used		fuel used	
		type	No	type	rate
Sayed Awadallah	Shoubra El Khima	SRF	3	mazote*	2.4 t/d
		Kettle	1	"	0.4 t/d
" "	" "	SRF	3	"	2.4 t/d
		Kettle+sh	2	"	0.7 t/d
" "	" "	SRF	3	"	2.4 t/d
		Kettle+sh	2	"	0.7 t/d
" "	10th Ramadan	SRF	2	"	2.4 t/d
" "	Hadyek el Kobba	kettle+sh	3	"	0.8 t/d
" "	El basatein	SRF	2	"	2.5 t/d
El-Amal	Shoubra el Khima	VSF	1	"	0.6 t/d
Abdel Karim	" "	SRF	1	"	0.8 t/d
		kettle+sh	3	kerosene	0.12 t/d
GEMET	El Tebbin, Cairo	SRF	3	mazote	2.4 t/d
El Amerya	El Amerya Ind.zone	SRF	1	mazote	0.8t/d
		VSF	1	mazote	0.6 t/d
Dr. Farouk	Kalyoub	SRF	2	mazote	1.5 t/d
El Hadeitha	"	kettle+sh	2	kerosene	0.9 t/d
un named	10th October	SRF	2	under erection	
Omar El morsi	Bab el shaerya	kettle	1	butanes	N.D
El Mahi	Hadyek el Kobba	SRF	1	mazote	0.4 t/d
		kettle+sh	2	"	0.8 t/d
Abdul Azim	El Gamalya	VSF	1	mazote	0.6 t/d
		SRF	1	"	0.8 t/d
		kettle	1	kerosene	0.5 t/d
Nabih Abd. hamid	Hadayek El Kobba	SRF	3	mazote	2.4 t/d
	Zawya El Hamra	kettle+sh	2	kerosene	0.8 t/d
Ahmed Ali		kettle	2	kerosene	0.8 t/d
Total t/d		**smelter:**			
		SRF+VSF	**27+3**		**52.4 t/d**
		kettle	**18**		**11.46t/d**
		shaping	**7**		variable

SRF = short rotary furnace VSF= very short furnace

* Now replaced with natural gas

Most lead smelters are located in Great Cairo (> 85%) and the minor part is located in Alexandria, and Kalyoub. According to the statistics of the year 1996, 30 lead smelters are nowadays available comprising the two variants of lead recycling furnace; namely, short rotary furnace SRF and very short furnace VSF.

3.2.2 Specific variants of kettle furnaces.

The term kettle furnace is devoted to a kettle made of cast iron weighing nearly 2.5 tons having the design similar to crucible of type C. It is used for remelting the hard lead ingots whereby the molten lead is treated with some chemical salts such as pyrite and elemental sulfur and may be lanced with steam or atmospheric oxygen. This is conducted to react with the undesirable metallic impurities or alloying components selectively to form slag. Heating is performed with normal burners using kerosene or natural gas. The maximum temperature of the molten lead is < 650 °C. The kettle furnace is normally fitted with a mechanical propeller for adequate and rapid stirring of the molten lead during refining.

3.3 The overall turnover of lead smelters.

About 32,000 tons of hard metal lead are annually recycled tons of hard lead is produced annually. This quantity is recovered from 60000 tons scrapped acid lead batteries (about 81% recovery efficiency of the available metal lead).

Hypothetically, the available annual production capacity of the already existing lead smelters amounts to about 40 000 metric tons. Table (8) shows the annual turnover of the existing lead industry, and table (9) shows the hard lead productivity of SRF and VSF:

Table (8) The annual turnover of lead smelter in Egypt.

Lead product	Plant location	The annual turnover			
		tons / y	% : total	unit price L.E	Sub. total million L.E
pure lead ingots (blocks, pigs and links)	G. Cairo El-tebbin	2560	8	3640	9.318
H.lead bullion	all sites	3840	12	2850	10.944
pipes & Fixtures	Cairo-Alexandria.	23500	73.4	3100	72.850
Sn,Sb-lead alloy		500	1.6	24000*	12.000
lead oxides		1600	5.2	4200	6.720
Total		**32000**	**100**		**111.832**

* about 30 % Sn

Table (9) The hard lead productivity of SRF and VSF:

Furnace type	Productivity, mt. /h
production capacity of SRF / h	1 - 1.18 mt
production capacity of SRF /d	16-16.4 mt
production capacity of SRF / y (70 w.days)	1120 -1150 mt
production capacity of SRFs / y	30240-31050
production capacity of VSFs / y	1260 - 1450
Production capacity of lead industry /y	**31500 - 32500**

3.4 The available production capacity as related to the specific variants of lead smelters.

Table (10) Shows the annual turnover production capacity of lead plants.

plant	No of furnaces	t pa/ furnace	total mt
Sayed awadallah	14 SRF	1120-1150	16500
El-Amal	1 VSF	500 -600	500
Abdel-karim	1 SRF		1150
GEMET	3 SRF		3500
Al-Amerya	1 SRF 1 VSF		1700
Dr. Farouk	2 SRF		2500
El Mahi	1 SRF		1150
Abdul Azim	1 SRF 1 VSF		1700
Nabih abdul hamid	3 SRF		3500
Total			**32 000**

It is seen that in Egypt approximately 2.74 million acid lead batteries are wasted annually. Average weight of this quantity is nearly 48000 metric tons. In the light of the existing recovery efficiency (about 81 %wt of the available metal lead or 53.33 % of the gross battery weight), the weight of produced hard lead amounts to 25500 m tons. Table (11) shows that type and quantity of the dust formed during the recovery process.

Table (11) Shows the type of dust and quantity of dust emission per year.

Furnace Type	No. of furnaces	Working capacity(t) F/a	Dust (g) / ton raw material	Total dust emission t/y	Deposition t/y
SRF	26	29120	2329.6	1630.72	698.88
VSF	3	1650	132	92.4	39.6
Kettle F	8	-	-	-	-
Total	**37**	**30770**	**2461.6**	**1723.12**	**738.48**

It can be seen that the main source for dust emissions rotary furnaces type. The quantity of the dust is highest with SRF and lowest with VSF. The average total weight of the dust emission about 1723 tons/ y whereby 30% (738t) of dust quantity deposited on the inner walls of the exhaust gas exit assembly.

Tables (12 through to 15) show the types, chemical composition, and level of outdoor, inside and from the stack emissions of a typical lead smelter without installing any abatement options.

Table (12) Types of Emissions of Lead smelter.

	Type of emissions in		
Industry	**air**	**industrial water**	**land**
Lead smelter	**solids**: $PbSO_4$, PbO_x, carbon, fly ash, metal lead fumes, oxides of antimony, Se, **gases**: SO_2, CO_2, CO, No_x, , Cl, organic gases	solids: $PbSO_4$, PbO_x ,carbon, fly ash, metal lead fumes, oxides of antimony, Se,	solids: $PbSO_4$, PbO_x ,carbon, fly ash, metal lead fumes, oxides of antimony, Se, hot water

The major components of these emissions are solid particles of meal lead, lead sulfate, iron oxide, and other metal oxides (antimony and selenium).

Table(13) Chemical analysis of outdoor emissions of a typical lead smelter without abatement options.

Item	**Wt. % of sample**		**Wt. % of sample**
Gaseous emissions:		**Solid emissions :**	
sulfur dioxide	4.02	carbon particles	6.65
carbon dioxide	9.12	lead sulfate	59.14
carbon monoxide	8.54	lead oxides	1.26
free acid	0.20	antimony oxides	0.87
water vapor	3.60	other metal oxides	3.45
other gases	1.27	free lead particles	1.88
total gases	**26.75**	**Total solids**	**73.24**
Total gases + solids			**100.0**

Table (14) Maximum limits of outdoor pollutants without abatement options.

Item	measured value	standard value	exposure period
Gaseous emissions:			
sulphur dioxide , μg /m^3	7 500	350 150 60	1 hr 24 hrs 1 year
nitrogen dioxide . μg /m^3	540	400 150	1 hr 24 hrs
carbon monoxide, mg /m^3	28	30 10	1 hr 8 hrs
Solid emissions :			
suspended particles, mg /m^3	60	0.150	24 hrs
lead sulphate, mg /m^3	3200		
lead oxides, mg /m^3	120		
antimony oxides, mg /m^3	10		
other metal oxides, mg /m^3	35		
Total susp. solids, mg /m^3	**3425**	**230**	24 hrs
		90	1 yr
total particulates mg/m3 (as specified by law 4/94)		**100**	

Table (15) Level of total indoor solid emissions as measured in a typical lead smelter, mg/m^3 without abatement option.

Site No. in the plant	sample No.	value, mg/m^3
1	1 2 3 mean	5.74 3.36 4.86 4.64
2	1 2 3 mean	10.1 7.45 8.5 8.7
3	1 2 3 mean	11.2 9.9 8.4 9.83
4	1 2 3 mean	6.45 5.55 6.2 6.06
all sites	range in mean /all sites	3.36 - 11.2 5.70

Table (16) represents the measured level of emission and fugitive dust coming out of the stack of a typical lead smelter using SRF type

Table (16) Level of total emissions from the stack of a typical lead smelter without abatement options.

Stack No.	Temp. °C	Exhaust gas, m3/h	solid in exh.gas g/m3	rate solid emission kg/h	lead conc. g/m3	SO2 in exh.gas ug/m3
furn. 1	260	3000	4.02	12.23	2.86	1271
furn.2	315	4200	3.85	14.9	2.22	1200
Mean	290		3.93	13.6	2.53	1235

The cost-effectiveness of abatement options for A typical lead smelter

Table (17) The different abatement options for monitoring emissions.

Option	**short term**	**long term**
Updating the burner	LS1	LS1
Replacing mazote with n.gas	LS2	LS2
installing cleaning system	LS 3	LS 3
Installing ventilation system	LS 4	LS 4
using new machines and updating plant technology	LS5	LS 5
No. of sub-options	8	22
relocation of lead smelter	-	LS 6
monitoring and inspection	LS 7	LS 7

Tables (18 & 19) show the technical target of the above mentioned abatement options and the changes that the firm would have to carry out respectively.

Table (18) The technical target of abatement options.

Option	No.	Technical target
Updating the burner	LS1	This includes improvement of combustion conditions of the used fuel, decrease of fuel consumption, and utilization of other cost-effective oxidizers
replacing mazote with kerosene or natural gas	LS2	reduction of solid and gas emissions
installing a cleaning system	LS3	Dust collection from stack and inside plant, separation of solids from waste water of cooling systems for recycling of the industrial water, the produced cake, and for monitoring temperature emissions.
installing ventilation system	LS4	regeneration of fresh air in the plant
using new machines and updating plant technology	LS5	- replacing manual operations in the existing plants by mechanical non-polluting means machines whenever possible and applying high technology of lead recovery - installation of a plant to recovery lead from collected dust
re-location of plants	LS6	removal of emissions in population and urban communities
monitoring and inspection	LS7	measurement and quality control the level of emissions inside the plant, in water and sanitary systems and in land throughout the working period /day

Table **(19)** The changes that the firm would have to carry out.

Option	**No.**	**Changes that the firm would have to carry out**
updating burner	LS1	Replacing old burner with new updated design suitable for using the same fuel or other light oil or natural gas. Install storage tanks, piping, fire fighting facilities, pressure gauges and electronic devices (2 labors)
replacing mazote with kerosene or natural gas	LS2	install two storage tanks, piping, fire fighting facilities, pressure gauges and electronic burners, temperature control panel (2 labors / furnace)
Installing cleaning system	LS3	hood, ducts and pipes, butterfly valves, different suction fans, wet scrubber, waste water treatment system (two storage tanks 150 m^3), 3 water pumps, filter press, chemicals preparation unit, gas sensors. (1-4 labors)*
Installing ventilation system	LS4	Window fans, gas ducts, collecting gas chamber, filter bags, suction fans, gas sensors, air conditioner, alkali bubbler, and elec.control panel (1-4 labors.)*
using new machines and updating plant technology	LS5	replacing the exizting manual operations with machined system and updating the production technology
re-location of plants	LS6	Install all abatement options LS1 through LS5
monitoring and inspection	LS7	would be carried out by subcontractors

3.5 Particle size analysis.

a) Dust composition.

The major part of the particles have the size < 0.106 mm. Table (20) shows that the size fraction > - 1.6 + 0.29 mm in diameter weighs 34.4 %. It is seen that ≈ 54 by weight of lead smelter dust is very fine and escapes as fugitive emissions. The coarser particles > o.29 mm are air born by the hot exhaust gas and deposits on the tunnel walls and its bottom as well.

However, deposited dust is frequently removed to accommodate easy flow of the flue dust towards the chimney. Escaped dust is now scrubbed using more sofasticated equipments applying wet technique.

Chemical analysis shows that metal content in dust is more or less the same 54 % Pb , 1.3 % Na by weight irrespective of the particle diameter (Table 21). It is also seen that the acid insoluble value (IR) decreases with the corresponding decrease of particle diameter. Table (22) shows the phase identification of chemical compound of dust.

Table (20) The weight percent of the particle size.

Size, mm	Wt. %	Cumm. Wt.% Pass
>8	3.86	100
>4. 76	2.87	96.14
>3. 36	3.33	93.27
>2. 5	2.72	89.94
>1. 65	5.93	87.22
>1.168	7.9	81.29
>0. 84	6.05	73.39
> 0. 589	2.94	67.34
>0. 295	6.58	64.4
>0. 147	1.71	57.82
>0. 106	2.12	56.11
<0. 106	53.99	53.99
Feed	100	

Table (21) The chemical analysis of the deposited dust.

Size, mm	Pb%	Dis.%Pb	IR.%	Fe%	Ca%	Na%	Mg%
>8	54.98	3.77	7.06	2.28	0.31	1.06	0.03
>4. 76	51.08	2.6	12.1	2.13	0.44	1.41	0.03
>3. 36	52.84	3.12	8.17	2	0.47	1.25	0.08
>2. 5	52.84	2.55	6.55	2.1	0.35	0.88	0.03
>1. 65	50.95	5.37	6.54	2.28	0.5	1.31	0.08
>1.168	53.64	7.53	6.56	2.41	0.31	1.28	0.05
>0. 84	52.69	5.66	6.79	1.69	0.38	1.34	0.05
> 0. 589	54.08	2.82	8.05	1.63	0.38	1.28	0.12
>0. 295	54.23	6.34	7.3	2.19	0.31	1.38	0.04
>0. 147	53.88	1.64	7.68	2.09	0.5	1.41	0.03
>0. 106	54.63	2.06	6.83	2.59	0.47	1.31	0.12
<0. 106	58.97	56.54	3.09	1.94	0.34	1.34	0.05
Feed	56.31	100	5.05	2.03	.36	1.31	0.05

Where Dis % Pb = Wt% / 56.31 x Pb% IR% acid insoluble recovery

Table (22) The phase identification of chemical compound of dust.

θ	D(A°)	I/I.	Identification compound
20.80	4.2705	72.16	$PbSO_4$
23.30	3.8177	44.84	$PbSO_4$
24.60	3.6188	18.04	$PbSO_4$
55.55	3.4864	29.63	Pb_2O_3, $PbSO_4$, PbO_2
26.70	3.3387	80.92	$PbSO_4$
27.70	3.2204	63.40	Pb_2O_3, $PbSO_4$
29.65	3.0129	100	Pb_2O_3, PbO, $PbSO_4$
30.01	2.9689	16.49	Pb_2O_3, PbO
32.40	2.7632	37.88	Pb_2O_3, PbO; $PbSO_4$, PbO_2
33.20	2.6984	42.52	$PbSO_4$
34.20	2.6218	12.88	$PbSO_4$
37.35	2.4076	15.97	PbO, $PbSO_4$
39.60	2.2758	17.52	PbO, $PbSO_4$
40.30	2.2379	5.41	PbSO4, PbO_2
41.10	2.1962	6.70	Pb_2O_3, $PbSO_4$
41.70	2.1659	26.54	Pb_2O_3, $PbSO_4$
42.40	2.1318	5.41	Pb_2O_3, $PbSO_4$
43.75	2.0691	89.43	$PbSO_4$
44.60	2.0316	56.70	PbO, $PbSO_4$
45.95	1.9750	20.61	Pb_2O_3, PbO, $PbSO_4$
47.80	1.9028	4.38	$PbSO_4$
48.40	1.8806	6.44	Pb_2O_3, $PbSO_4$, PbO_2
50.90	1.7940	15.97	Pb_2O_3, PbO, $PbSO_4$
52.60	1.7399	9.53	Pb_2O_3, PbO
53.80	1.7039	16.23	Pb_2O_3, PbO, $PbSO_4$
55.45	1.6570	7.21	Pb_2O_3, $PbSO_4$
56.70	1.6234	18.55	Pb_2O_3, PbO, $PbSO_4$
57.10	1.6130	11.85	Pb_2O_3, $PbSO_4$
58.80	1.5704	6.18	Pb_2O_3, $PbSO_4$, PbO_2

Pb_2O_3 No. of card 33- 331

PbO No. of card 5- 570

PbO_2 No. of card 25- 447

$PbSO_4$ No. of card 36- 1461

b) Composition of the slag.

The slag was obtained from five positions of the slag pool, ground and then classified with respect to particle size. Tables (23-25) show the metal content as a function of particle size.

Table (23) Composition of slag sample having -1000+400μm in diameter.

	weight % 1st position	weight % 2nd position	weight % 3rd position	weight % 4th position	weight % 5th position	weight % mean
Pb	20.72	20.716	20.238	19.36	20.587	**20.324**
Sb	0.707	0.613	0.6559	0.6559	0.644	**0.659**
Fe	44.99	51	44.43	44.43	48.07	47.23
Si	16	14.7	17.7	17.7	15.9	16.6
Ca	2.7	2.8	2.5	2.5	2.6	2.74

Table (24) Composition of slag sample having -400+63 μm in diameter

	weight % 1st position	weight % 2nd position	weight % 3rd position	weight % 4th position	weight % 5th position	weight % mean
Pb	17.71	18.438	18.587	17.621	17.729	**18.017**
Sb	1.03	0.2457	0.2667	0.957	0.5396	**0.6078**
Fe	41.09	47.28	46.51	43.72	43.25	44.37
Si	20.85	20.55	18.43	20.11	18.97	19.78
Ca	2.35	2.53	2.55	2.42	2.6	2.49

Table (25) Composition of slag sample having -63μm in diameter.

	weight % 1st position	weight % 2nd position	Weight % 3rd position	weight % 4th position	weight % 5th position	weight % mean
Pb	14.626	14.386	14.047	14.182	14.507	**14.349**
Sb	0.711	0.573	0.8571	0.2326	0.8798	**0.6507**
Fe	40.26	35.46	35.3	38.72	39.09	37.766
Si	22	23.47	24.18	22.92	21.84	22.882
Ca	2.91	3.266	3.74	2.998	2.89	3.160

It was seen that lead and iron content in the slag samples decreased with the decrease of particles size. Lead and iron content amounted to 20.3 % and 47.2 % by weight respectively with coarse particles having –1 mm +0.4 mm. This amount decreased to 14.4 % and 37.76 % by weight with fine slag having – 63 μm in size. The content of silica and calcium displayed a mirror image to that of lead and iron. Silica increase from 16.6 % to 22.88 % by weight with coarse and fine particles respectively. On the other hand, antimony content was nearly constant for all the slag samples amounting to ≈ 0.65 % by weight.

Figures 17 through 19 demonstrated the X- ray microprobe spectrum pattern of the slag fractions.

Plates 8 through 13 show a magnified photograph of slag fractions. Plates 14 & 15 were for dust samples.

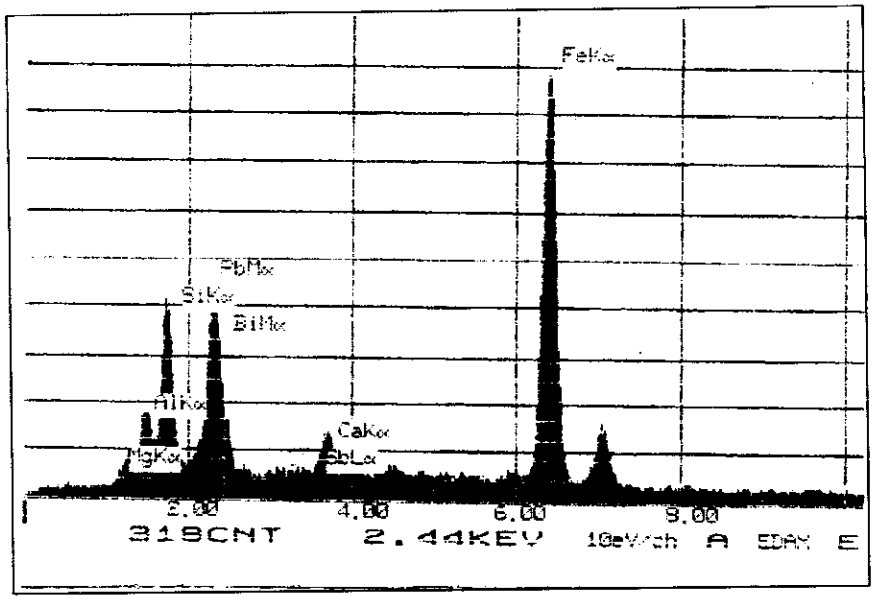

Fig. 17 X- Ray microprobe of slag fraction –1000+400 µm.

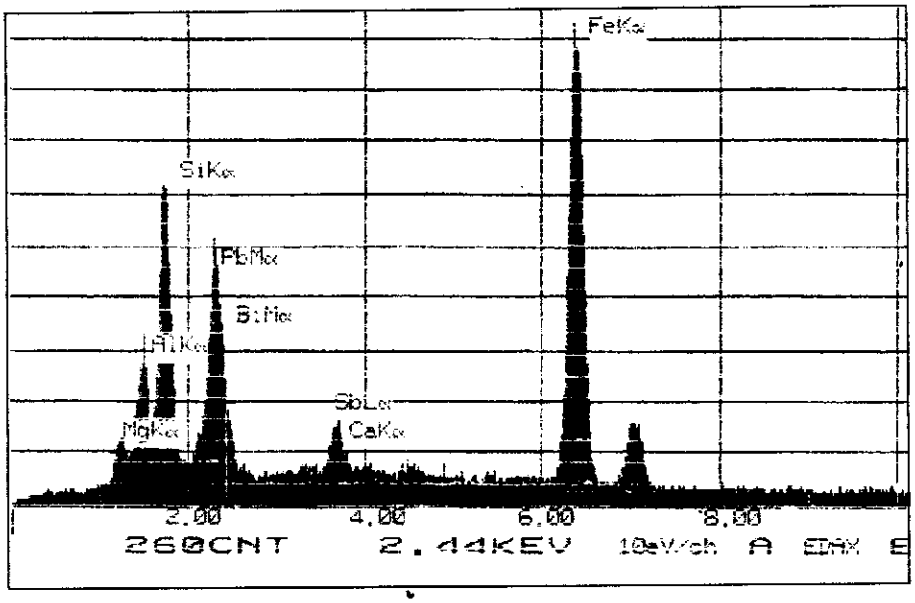

Fig. 18 X- Ray microprobe of slag fraction +400-63µm.

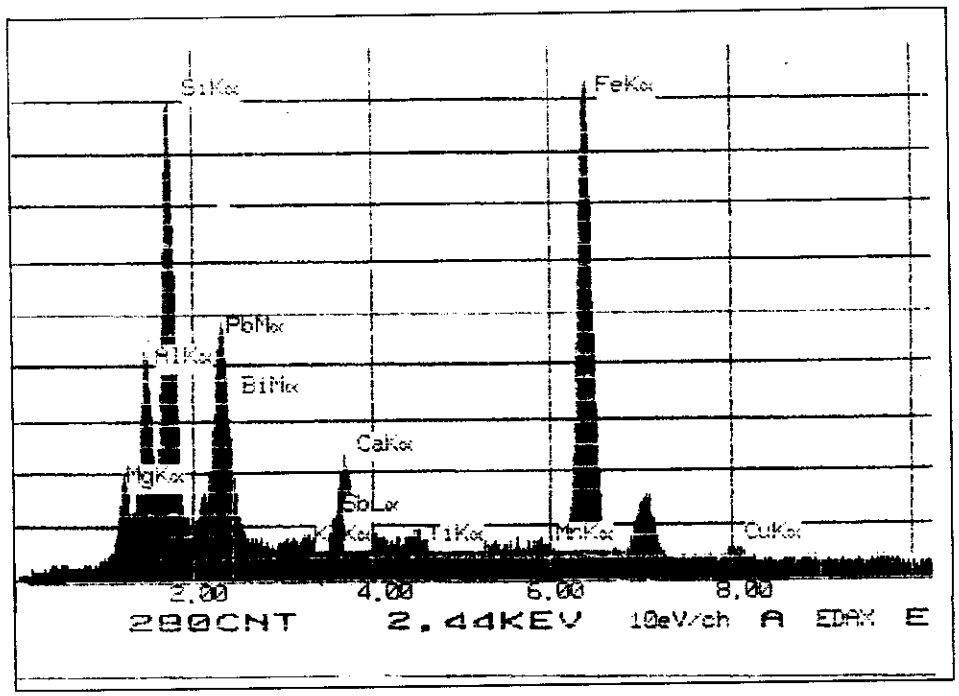

Fig. 19 X- Ray microprobe of slag fraction –63 µm.

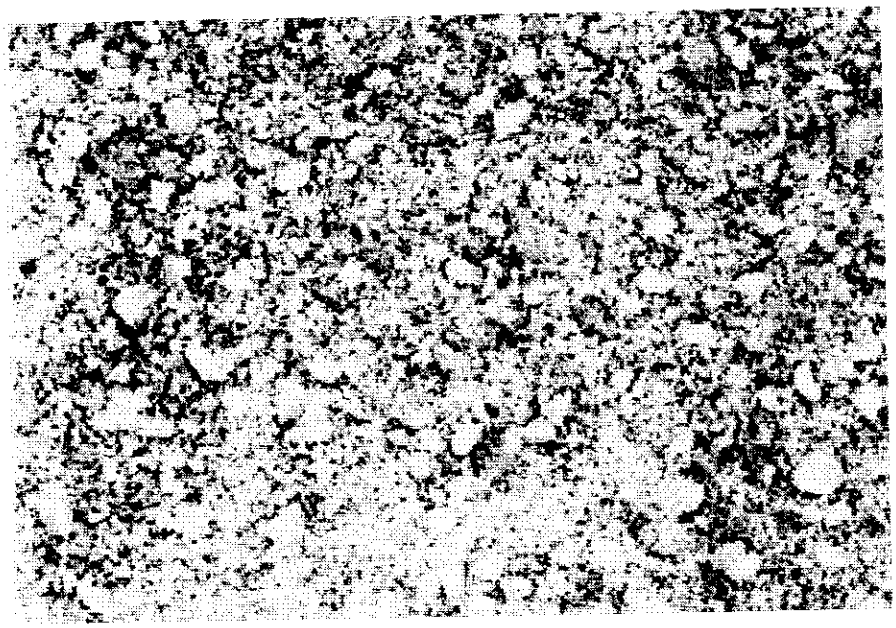

Plate (8) A photograph of fraction -1000+400µm (magnified 25 time).

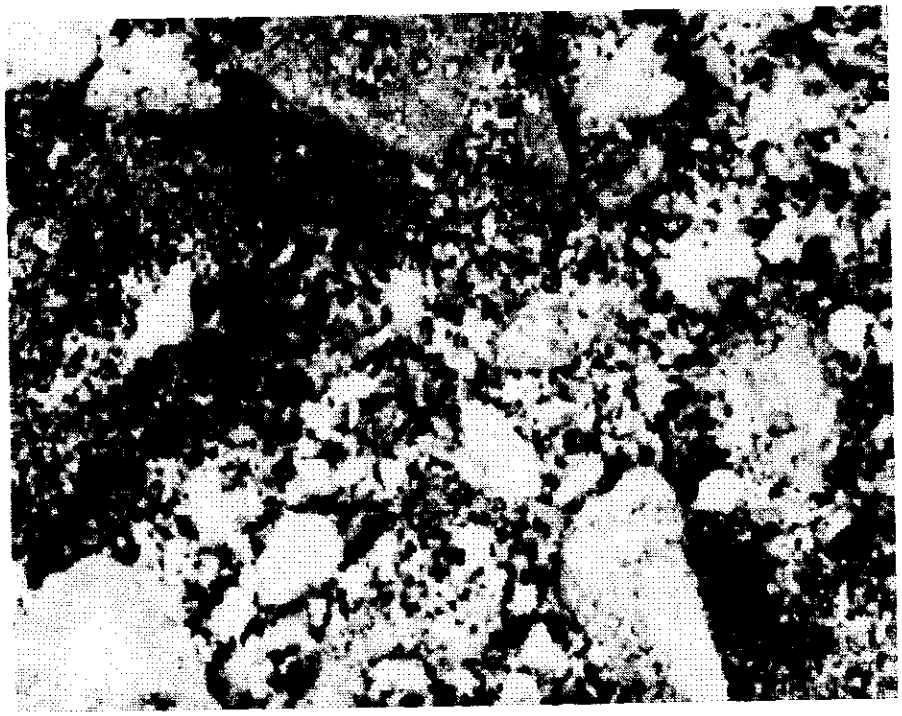

Plate (9) A photograph of fraction -1000+400µm (magnified 250 time).

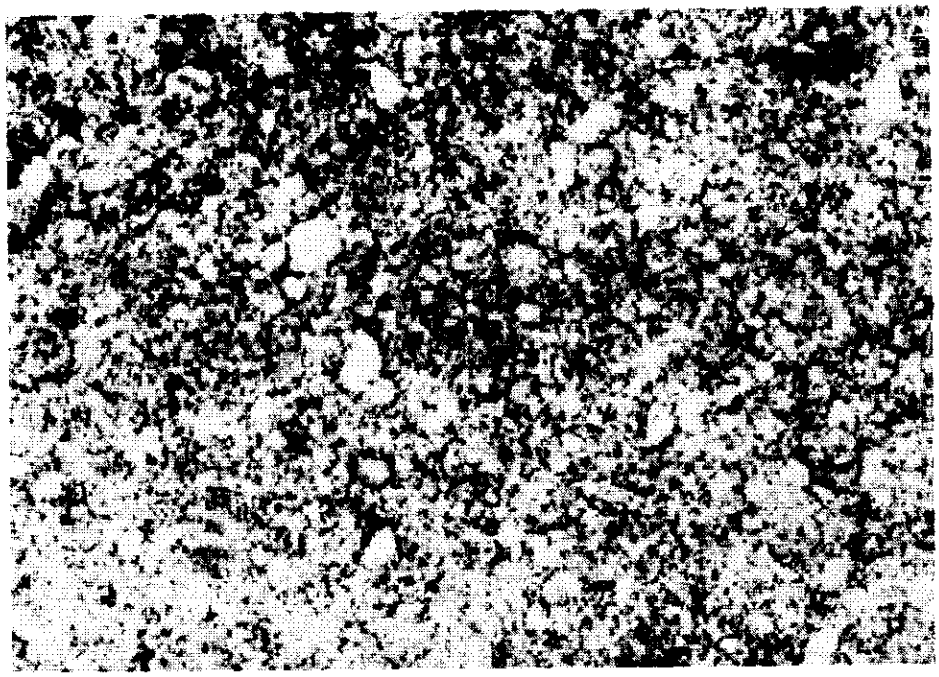

Plate (10) A photograph of fraction –400+63µm (magnified 25 time).

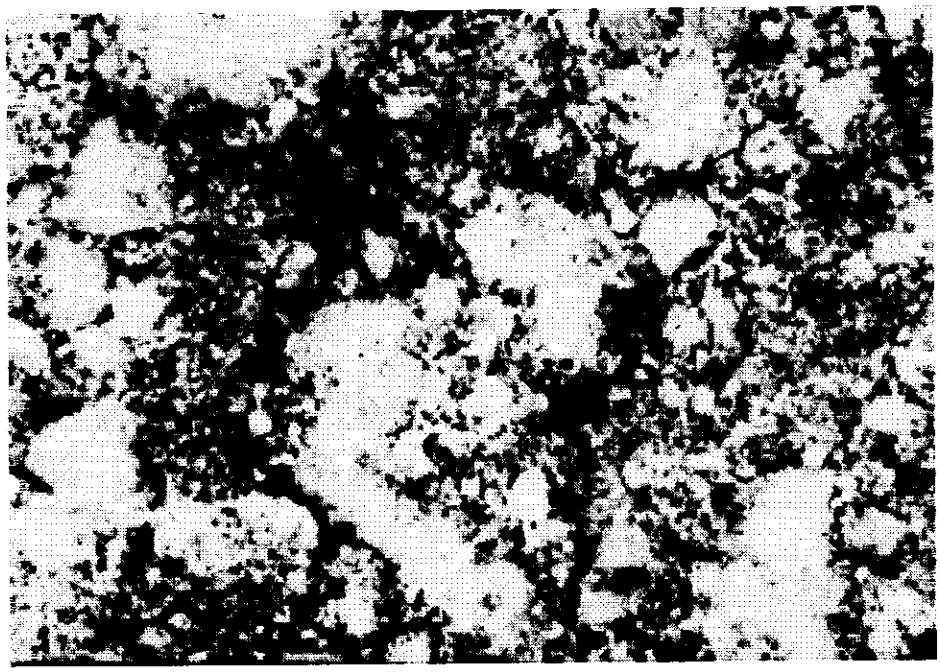

Plate (11) A photograph of fraction –400+63µm (magnified 250 time).

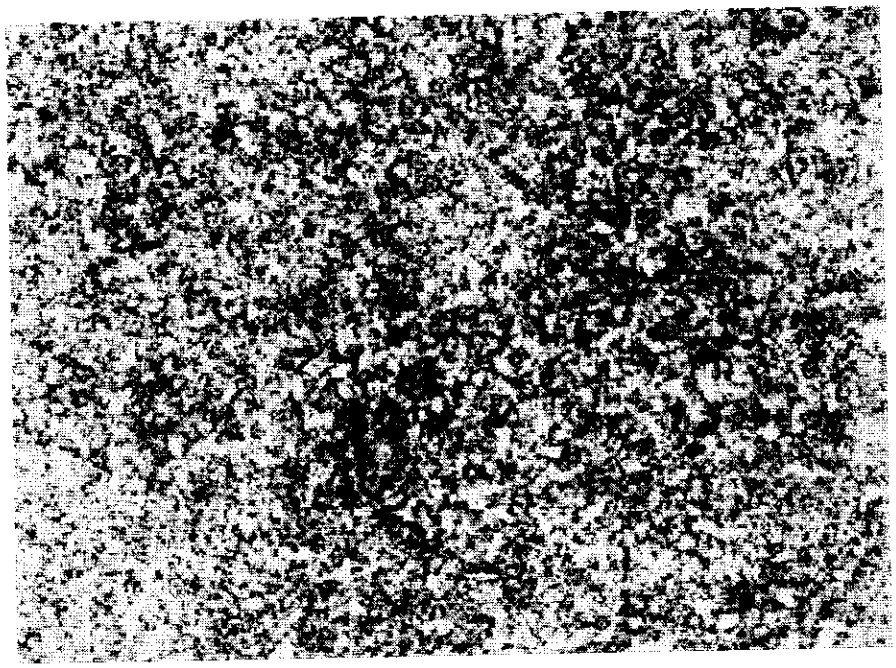

Plate (12) A photograph of fraction -63µm (magnified 25 time).

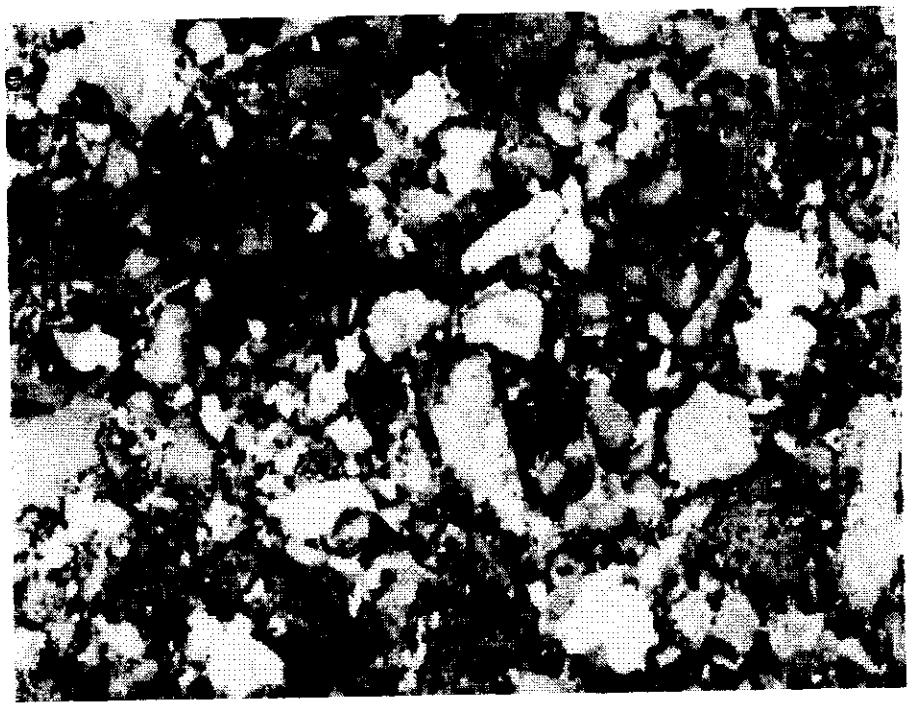

Plate (13) A photograph of fraction -63µm (magnified 250 time).

Plate (14) A photograph of Dust (magnified 25 time).

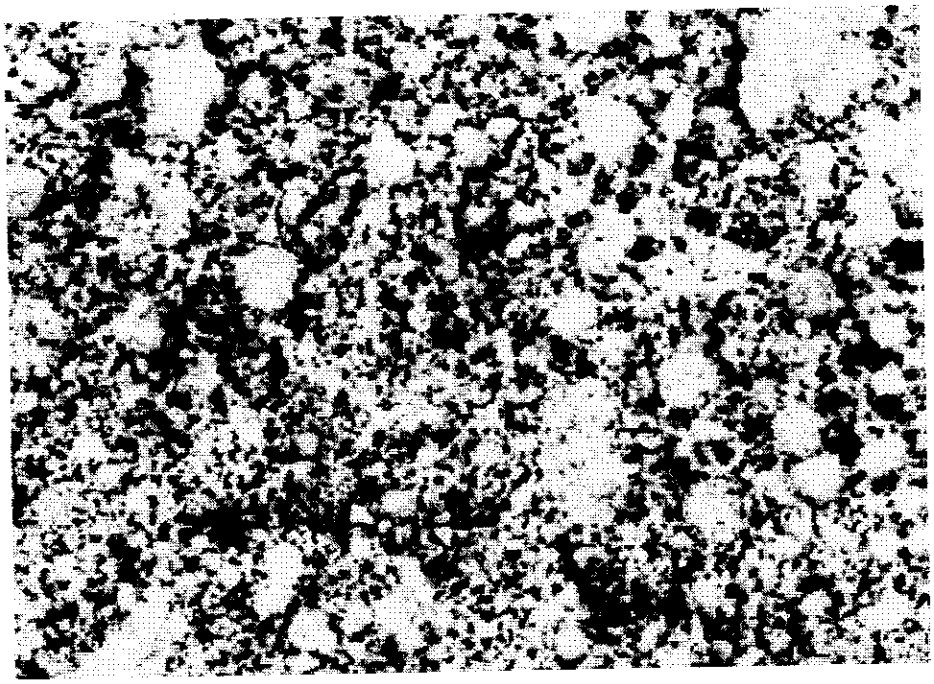

Plate (15) A photograph of Dust (magnified 250 time).

3. 6 Dust collection.

Table (26) illustrates the characteristics of the three filtration materials used in this work.

Table (26) Characteristics of the tested filtration materials.

Property	Filtration material		
	Al wool	**Steel wool**	**Ceram. fiber**
Real density, kg/m^3	2702	8790	2450
acid resistance	reacts	reacts	resistant
oxidation resistance	weak	weak	excellent
fiber cross section	rectangular	rectangular	circular
fiber diameter, mm	0.1-0.15	0.2-0.25	0.15-0.3
surface roughness	rough	rough	smooth
surface area ,m^2/kg	1.72	0.53	1.2

It was seen that the filtration materials covered a wide spectra of density, chemical stability and surface area. Ceramic fiber chemically resistant to acid and has an intermediate surface area as compared to the other two metallic materials. Figure 20 shows the effect of compression force on the apparent density of these materials. It is seen that with metallic wool, an increase in density takes place with increases in compression force. With ceramic fibers, the density change is less significant approaching a maximum and constant magnitude at > 7.5 MPa. Densification of the filtration materials increases in the order steel wool > aluminum wool > ceramic fibers.

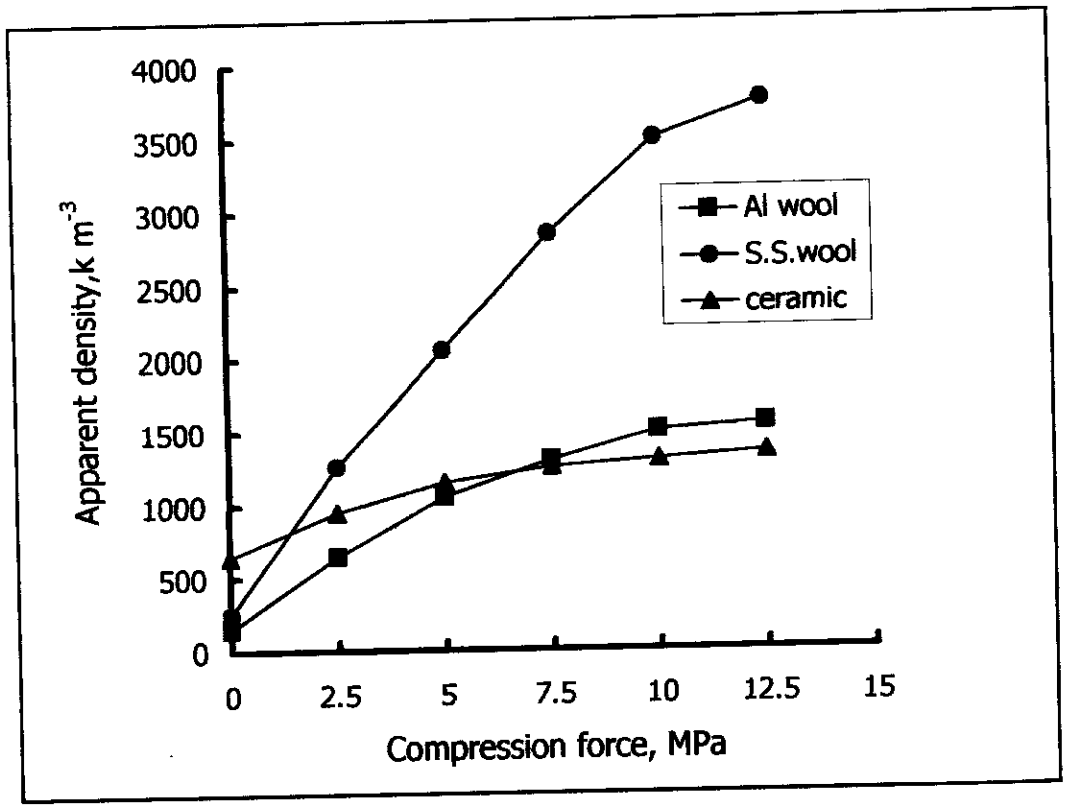

Fig. 20 Effect of compression force on the apparent density of filtration media made of different materials.

Figure 21 shows the total porosity change of the filtration materials as affected by compression. It can be seen that a gradual decrease in porosity value takes place with increase in compression force. Porosity changes in the order steel < ceramic fibers < aluminum whenever compression is compared at >7.5 MPa. Porosity measurement of the pore system is given in figure 22. It can be seen that the pore system of the filtration materials has a size > 10 microns for both the uncompressed metallic wool and ceramic fibers. With compression, a pore system having a narrower pore size is gradually achieved. With compressed steel wool only a minor portion of the pore system are mesopores (> 1 < 10 microns) whereas the major portion is macropore in size (> 10 microns).A higher volume percentage of mesopores is seen with aluminum wool prepared under the same conditions. However, with ceramic fibers micropores having a pore diameter < 1 micron are detected. The portion of meso- and macropores are higher and lower respectively as compared to the metallic wool samples.

Figure 23 shows the gas permeability as affected by gas pressure. It can be seen that ceramic fibers possess higher gas permeability as compared to the other two materials. Figure 24 shows the cleaning efficiency the flue gas (ζ), carrying lead sulfate solid particles as affected by the particle diameter δp. It can be seen that ζ value increases with increase in δp. For one and the same δp value, ζ, decreases the order ceramic fibers > aluminum wool > steel wool. Figure 25 shows the effect of gas velocity on ζ,. It can be seen that ζ, increases slightly with the corresponding increase in gas velocity passing through a maximal at 0.5 m/s.

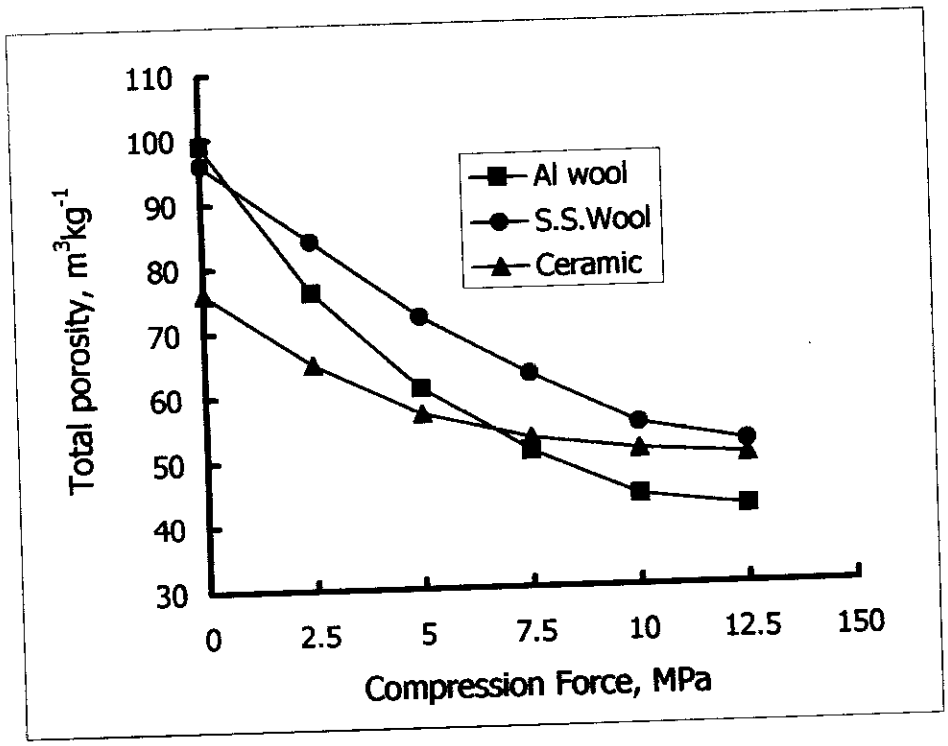

Fig. 21 The total porosity of the filtration pad as affected by compression force.

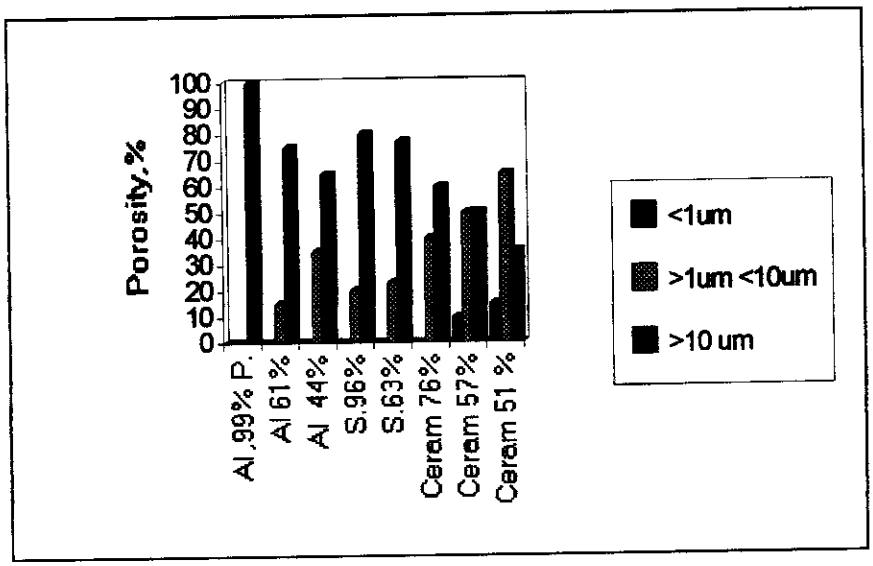

Fig. 22 The porosity distribution of the filtration materials.

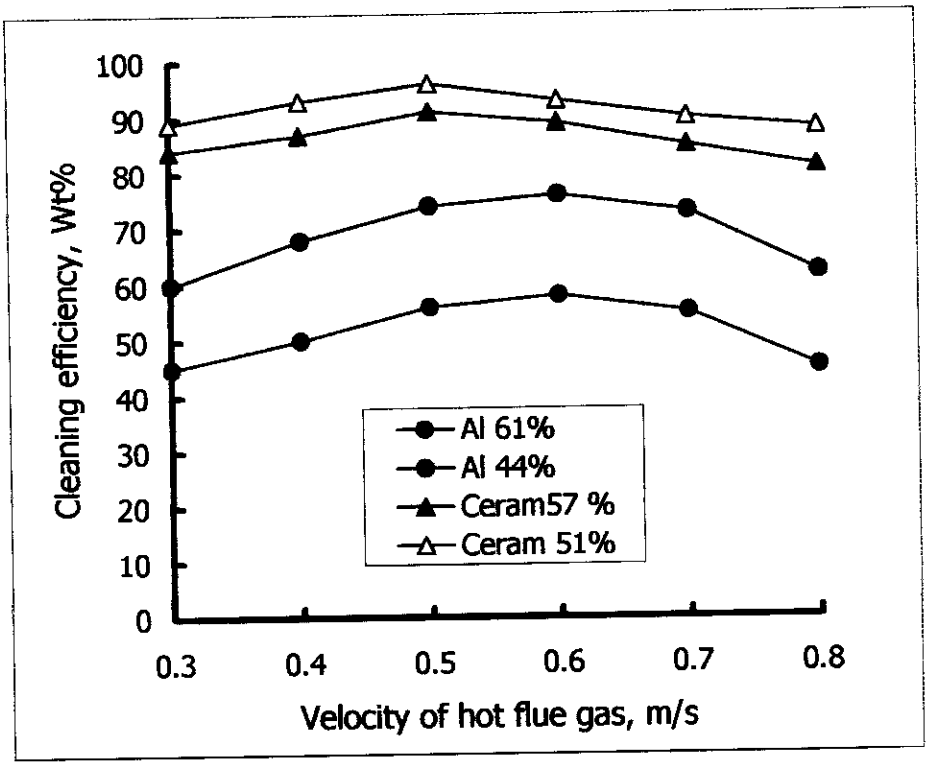

Fig. 25 Effect of velocity of hot flue gas on the cleaning efficiency of the assembly.

Figures 26 and 27 show that ζ, increases with increasing the ratio of both the diameter/ length and thickness of the filtration material /height of compartment, of the cleaning device. Maximum ζ, value is at 0.25 and 0.8 with the former and latter parameter respectively.

Figure 28 illustrates that the temperature of the outlet gas T_{go} decreases as the inlet gas velocity increases passing through a minima at 0.5 m/s. It may be noted that with aluminum wool, Tgo is comparatively higher than that acquired with ceramic fibers. Figure 29 shows that the theoretical T_{go} value is higher than that experimentally determined with any of the filtration material used by nearly 28 %.

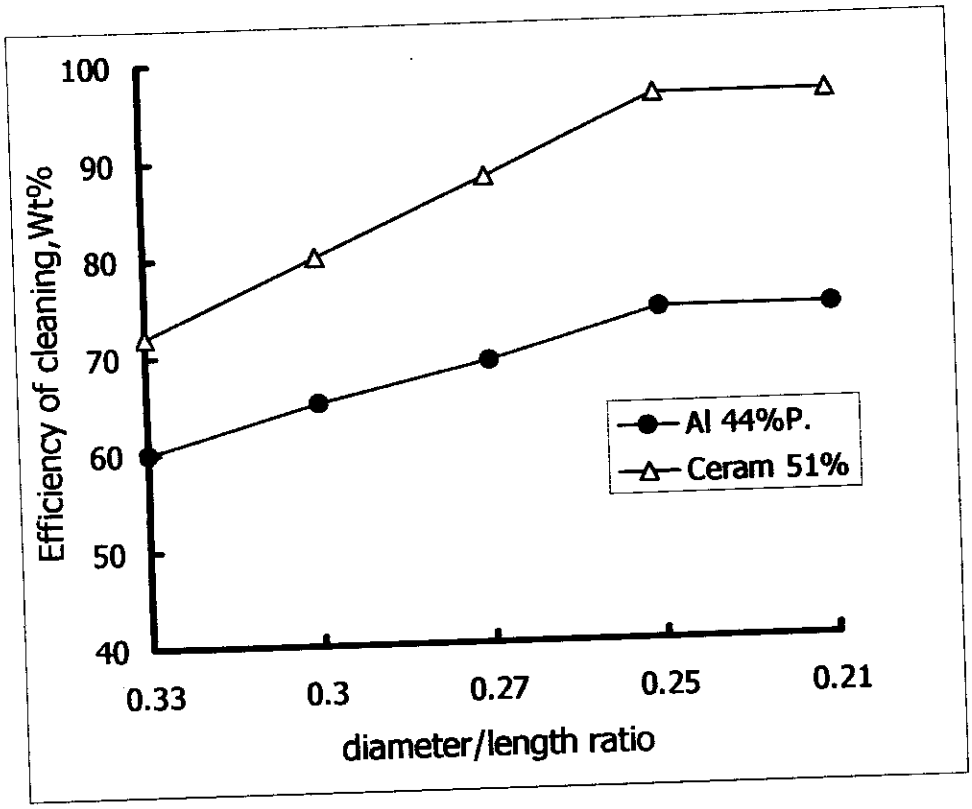

Fig. 26 Effect of diameter/length ratio of the assembly on its cleaning efficiency.

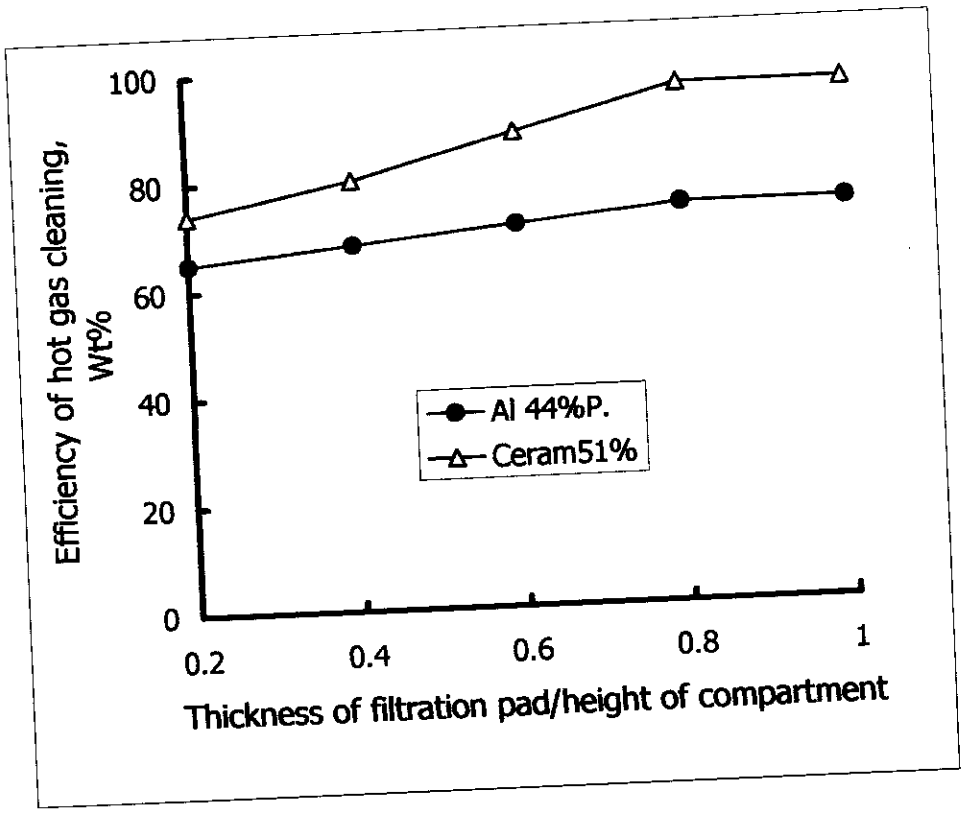

Fig. 27 Effect of filtration pad on cleaning efficiency of the assembly.

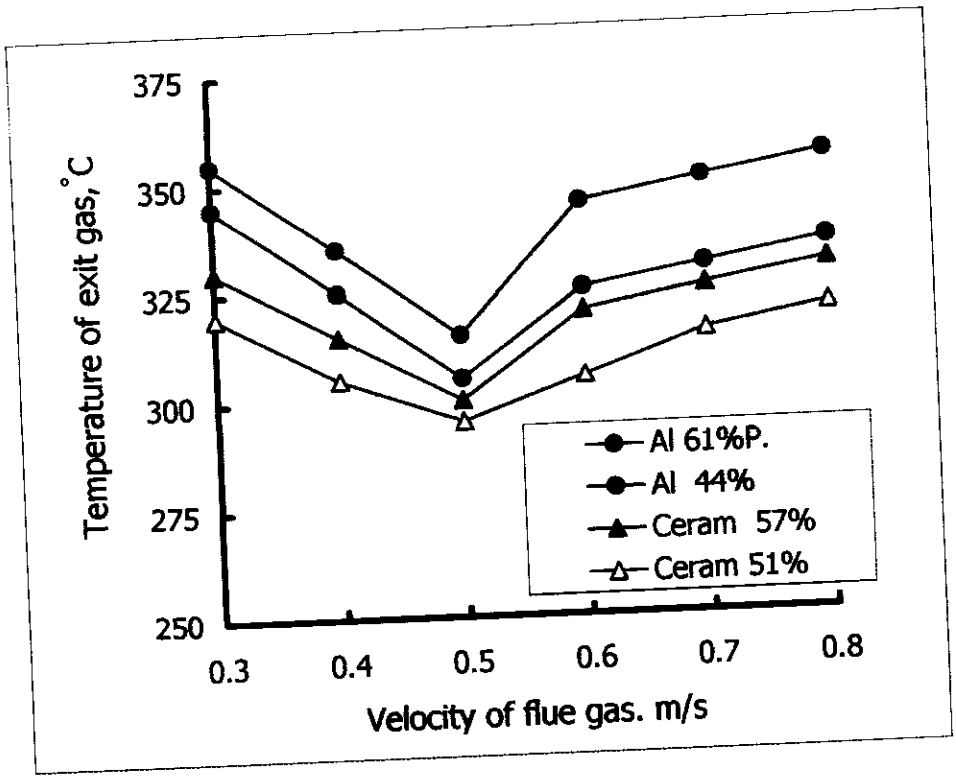

Fig. 28 Effect of flue gas velocity on the exit gas temperature (inlet gas T= 450°C, particle diameter >10 um <63 um).

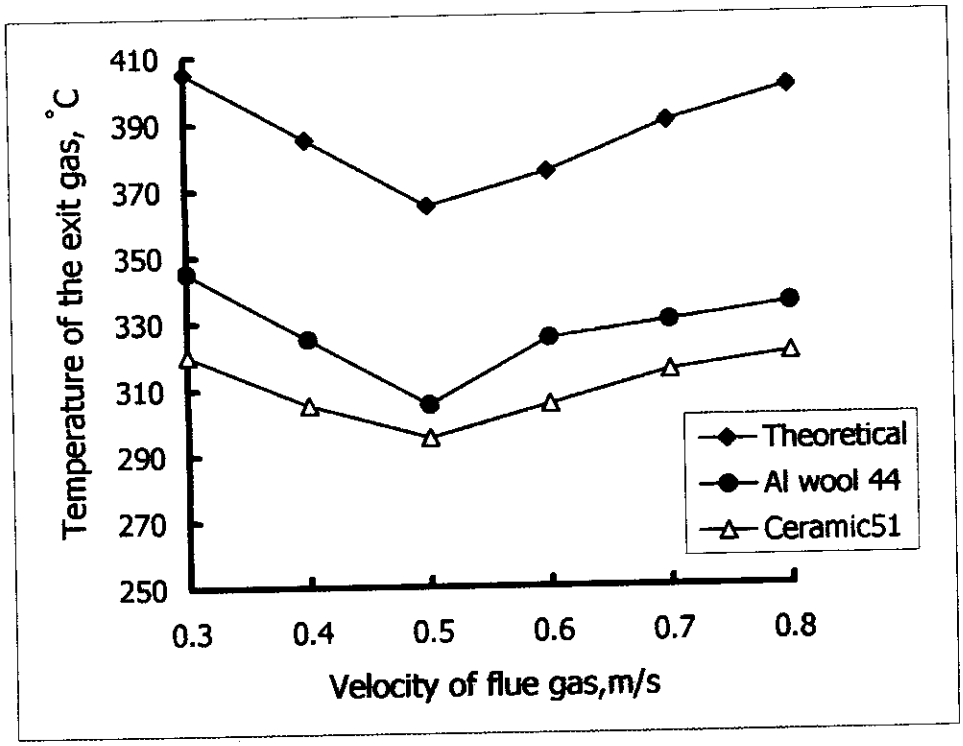

Fig.29 Temperature of the exit flue gas as calculated theoretically and experimentally measured (conditions as given in Fig. 26).

3.7 Conversion of lead dust to lead carbonate.

As for as lead metal recovery is concerned lead dust was converted to lead carbonate. The dust was composed of lead sulfate and lead oxides. The two compounds were separated from each other by dissolving the dust sample in ammonium acetate solution. Lead oxide readily dissolved, figure 30 shows the extent of solubility of synthetic lead oxide (PbO) and lead sulfate ($PbSO_4$) in 1M NH_4COOCH_3 at different temperatures. It is seen that lead oxide dissolved completely [100%] at 80 ° C in 1 M ammonium acetate. However 30 % of lead sulfates dissolved. In other words 70 % of lead dust was dissolved in ammonium acetate to separate lead sulfate from lead oxide. Experimental results solved that about 70 % of the dust was insoluble i.e. separated lead sulfate.

Figure 31 shows the activation energy value of the dissolution criterion. The ΔE value as computed from Arrhenius plot amounted to 1.35975, 2.2555 KJ / mol for both lead oxide and lead sulfate in ammonium acetate respectively. This was taken to suggest that the dissolution step is physical criteria rather than a chemical reaction.

The dissolved lead acetate was reacted with sodium carbonate solution to yield lead carbonate. Conversion of lead acetate to carbonate was examined at different temperatures up to 70 ° C. Figure 32 through 34 demonstrated the extent of carbonation. In Figure 32, it was seen that increasing the temperature of the reactants enhanced the extent of conversion of lead acetate to carbonate took place at 60 ° C. In Figure 34 it was found that using 1M stochiometric ratio of sodium carbonate at 25 ° C achieved the highest extent of carbonation (100%) after 50 hours of carbonation.

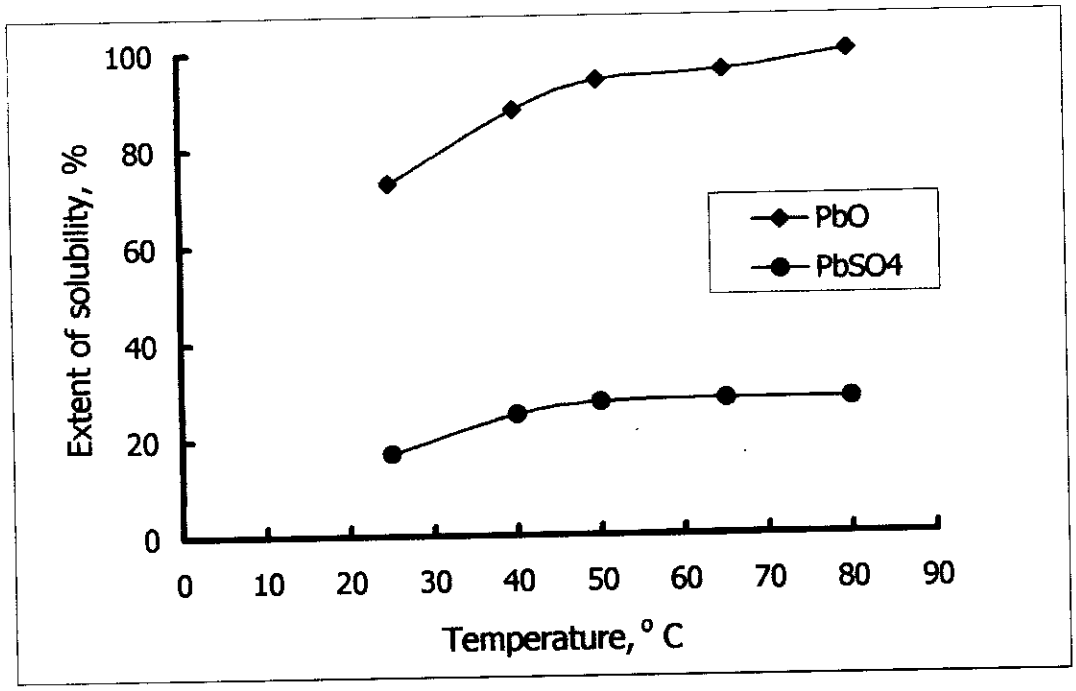

Fig. 30 The extent of solubility of synthetic lead oxide (PbO) and lead sulfate ($PbSO_4$) in 1M NH_4COOCH_3 at different temperatures.

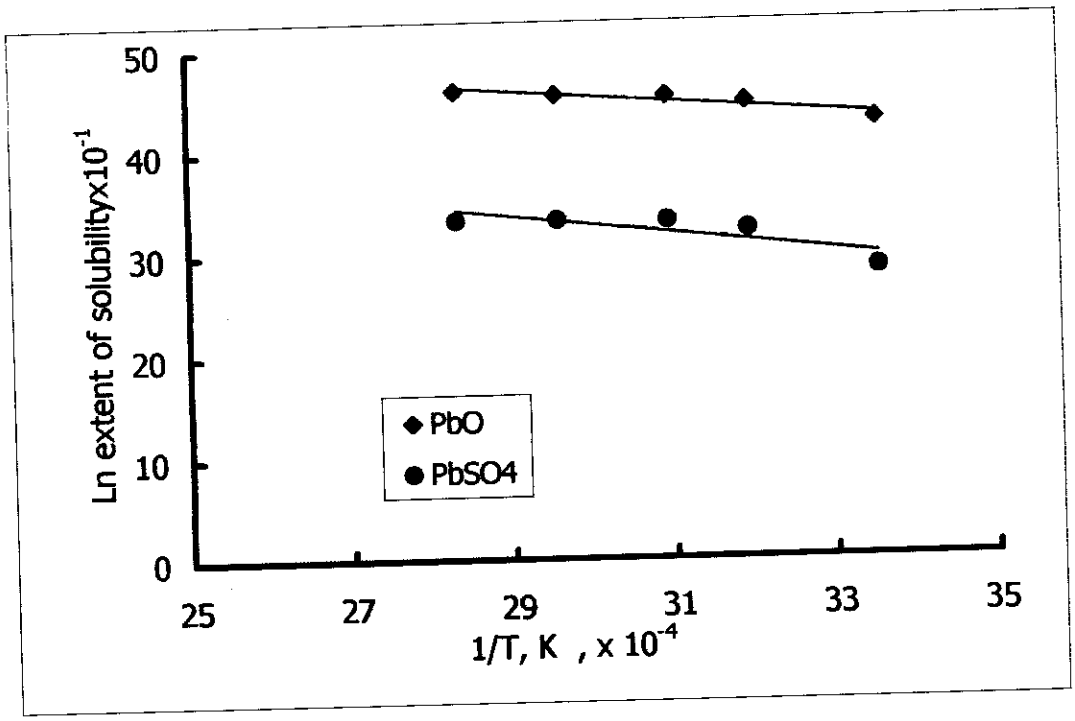

Fig. 31 The activation energy value of the dissolution criterion.

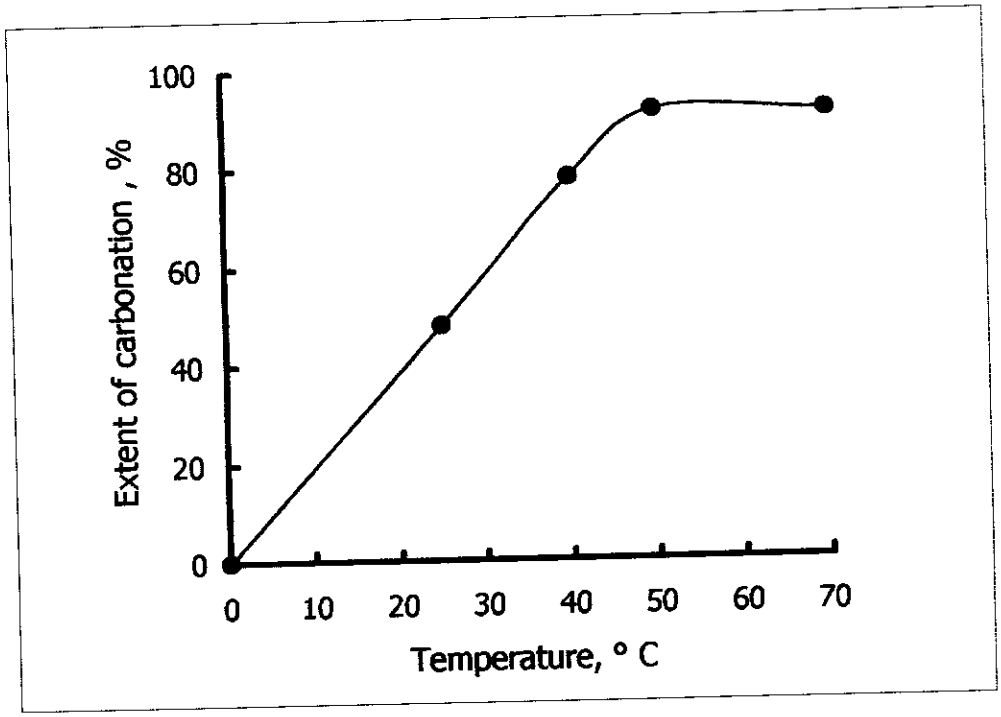

Fig.32 Effect of temperature on the extent of carbonation at (1:1 stichiometric, 2hr., and stirring150rpm).

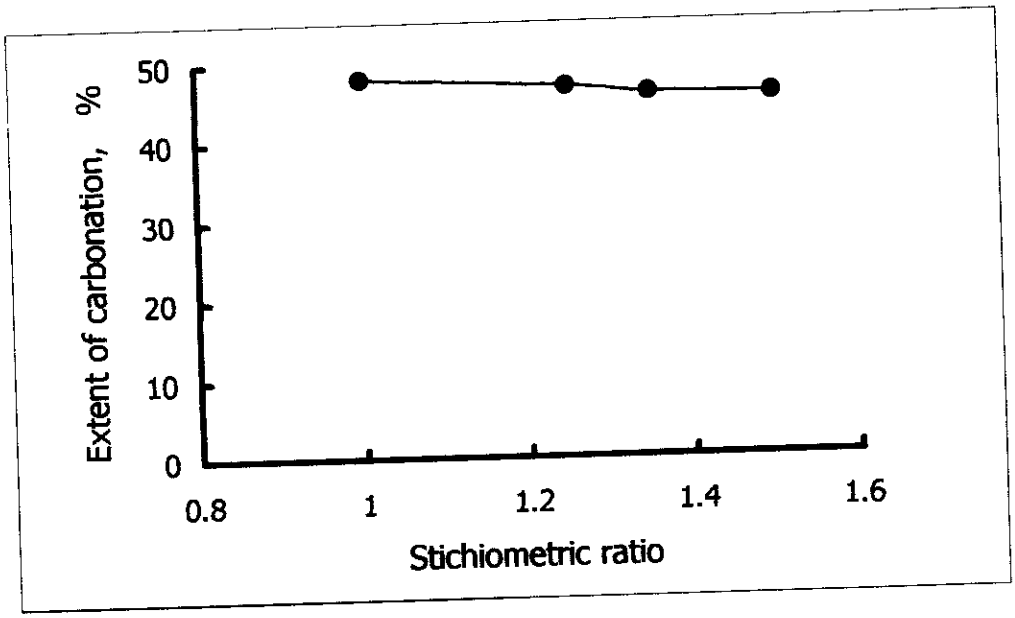

Fig. 33 Effect of stichiometric ratio of Na_2CO_3 on the extent of carbonation for 2hr.,at room temperature (stirring150rpm).

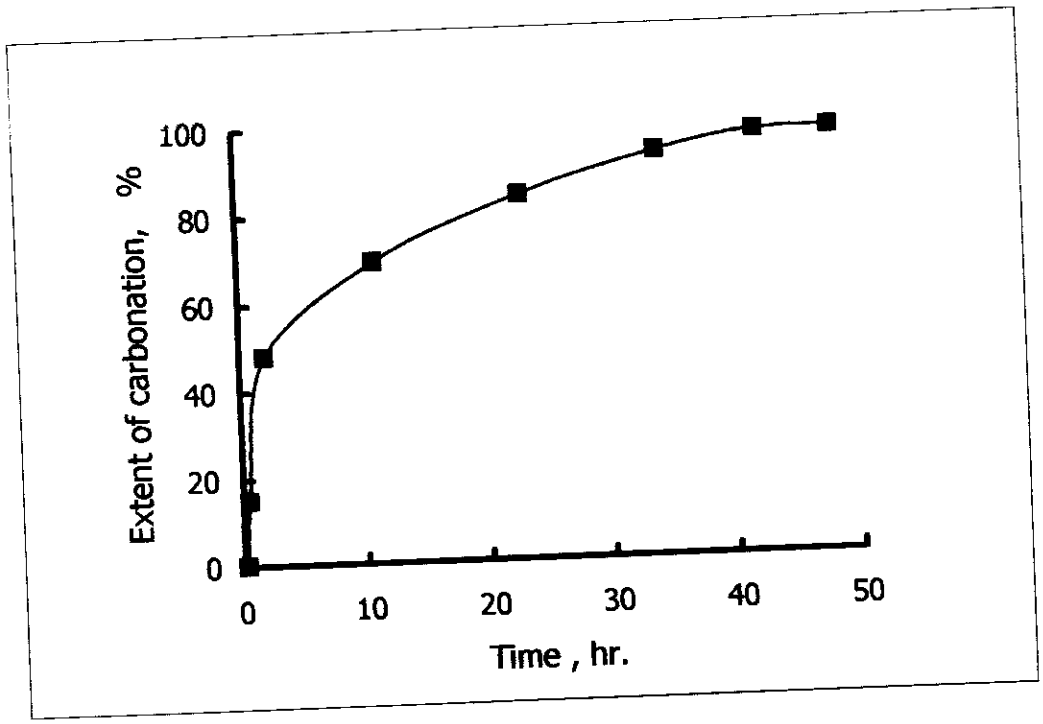

Fig. 34 Effect of time on the extent of carbonation at (1:1 stichio-metric ratio, room temperature, and stirring150rpm).

3.8 Optimum conditions pelletization and recovery of dust using carbon reduction.

Figure 35 shows the uncontrolled fugitive solid emissions (FSE) emission as a function of smelting temperature for powder and pellets having various particle diameters. FSE emission level increases linearly with increases in smelting temperature. FSE emission level caused by smelting of battery paste powder is relatively higher than that caused by smelting of the pelletized paste. FSE emission level monitored at 1000°C and 1200°C using powder paste amounts to 2750 and 3510 $\mu g/m^3$. The FSE level measured with pellets having 10mm diameter amounts to 960 and 1150 $\mu g/m^3$. Therefore, 65-67% of the FSE level is reduced due to pelletizing the battery paste. However, all these levels do not comply with the level specified by the law 4/94 (100ug/m3).

Figure 36 shows the controlled FSE using a wet scrubber for gas cleaning. The monitored FSE level is found acceptable with the constraints given by the law. However, the scrubbed solids are recycled for the pelletizing step.

Figure 37 shows the mechanical strength of the pelletized lead dust as a function of content using different particle size of the used materials. The mechanical strength value increases gradually with increase in molasses percentage approaching a maximum value with ≥ 12.5 % molasses. The standard strength is achieved with pellets having a diameter ≥ 10 mm in diameter. Figure 38 shows the recovery percentage of metal lead (W_{mr}) as a function of the smelting temperature using the composition shown in table (5). It is seen that W_{mr} increases with increase in the temperature up to 1100°C.

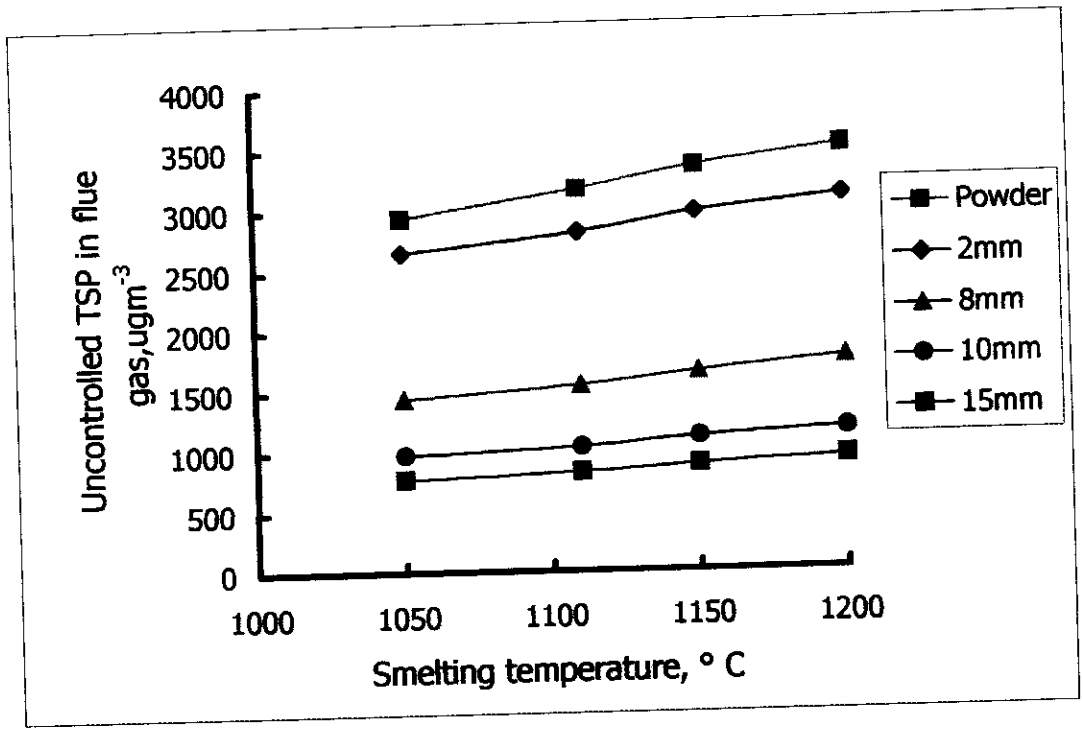

Fig.35 Uncontrolled TSP level ($\mu g/m^3$) as affected by smelting temperature using powder and pelletized dust.

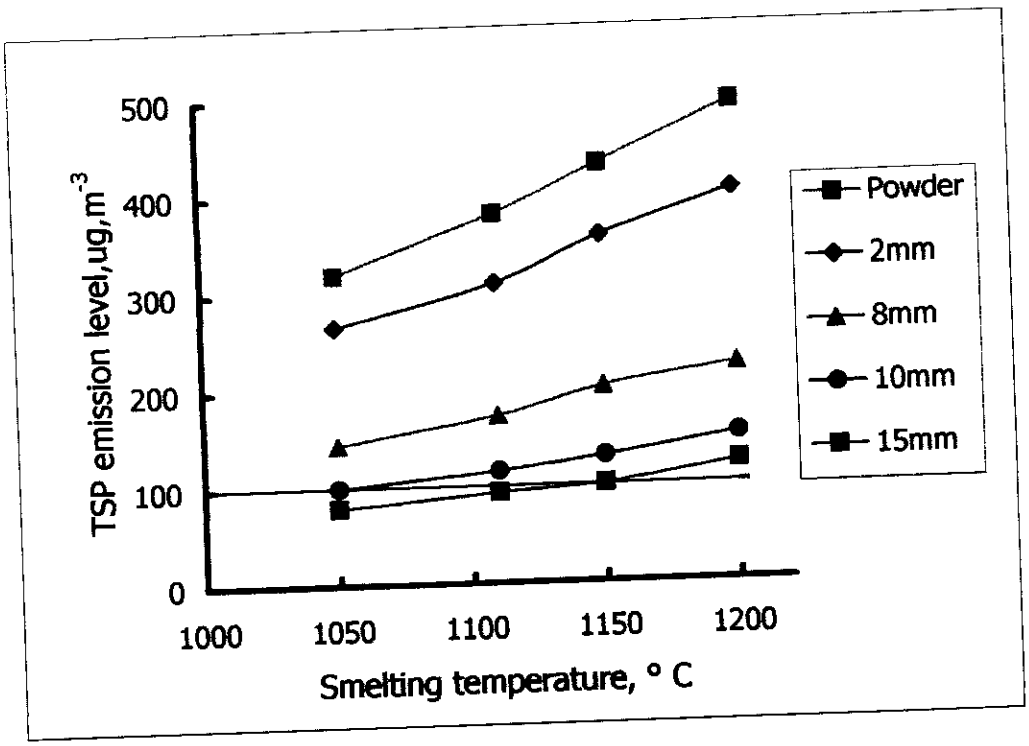

Fig.36 Controlled TSP emission level of powder and palletized dust as a function of smelting temperature.

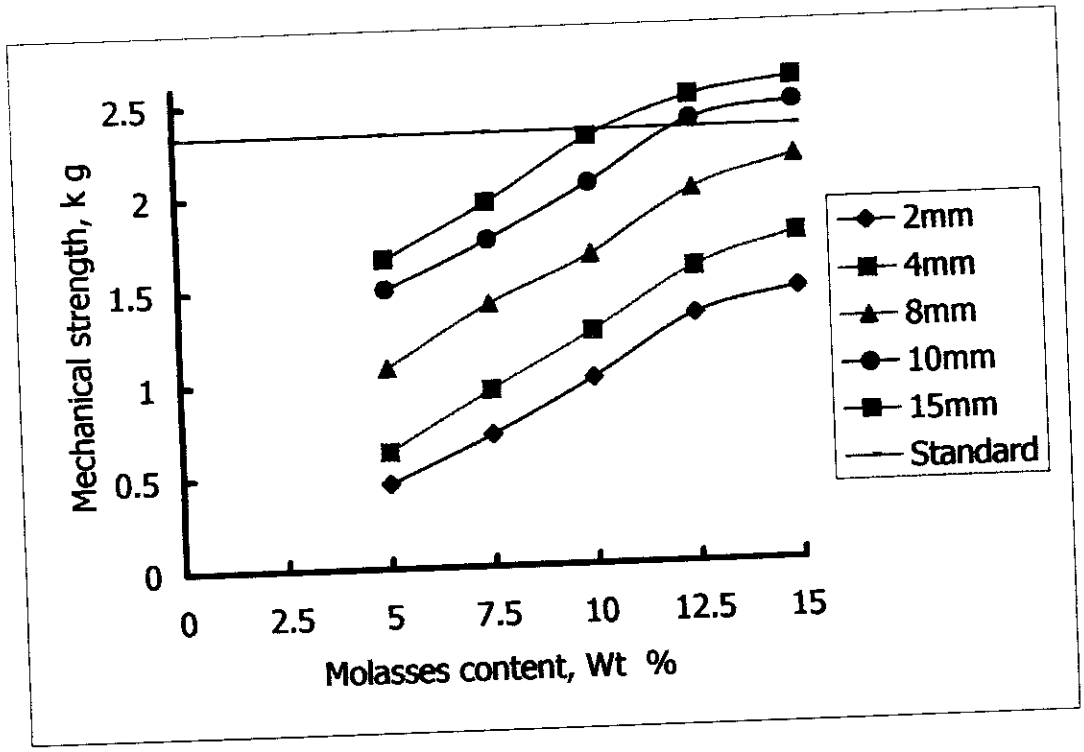

Fig.37 The mechanical strength of palletized dust as affected by molasses content.

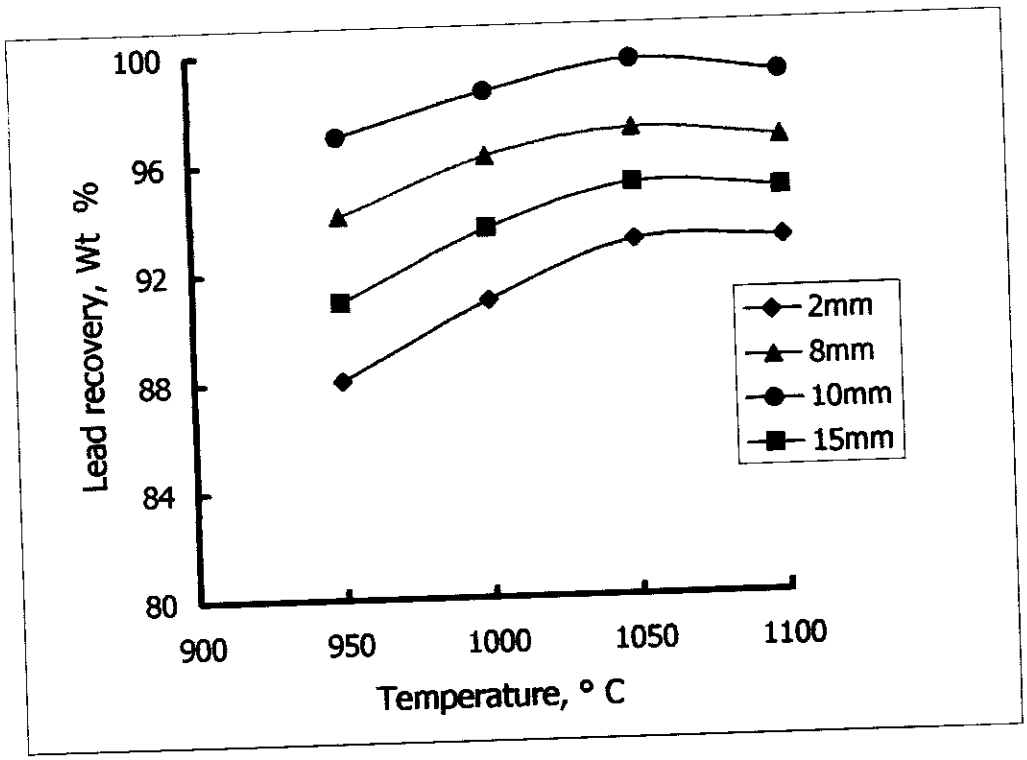

Fig.38 The recovery percentage of metal lead as a function of smelting temperature.

The maximum W_{mr} value is achieved at 1050°C., pellet having 10 mm in diameter acquires the highest W_{mr} value (99.6). Figure 39 shows that the lead recovery increases with increases in particle diameter of the pellets passing through a maximum value with pellets having 10 mm in diameter. The lower W_{mr} value is determined with particles having larger diameters. Figure 40 the Arrhenius plot of the thermal recovery of metal lead from the prepared pellets. The average ΔE value amounted to 1.78678 KJ/mol.

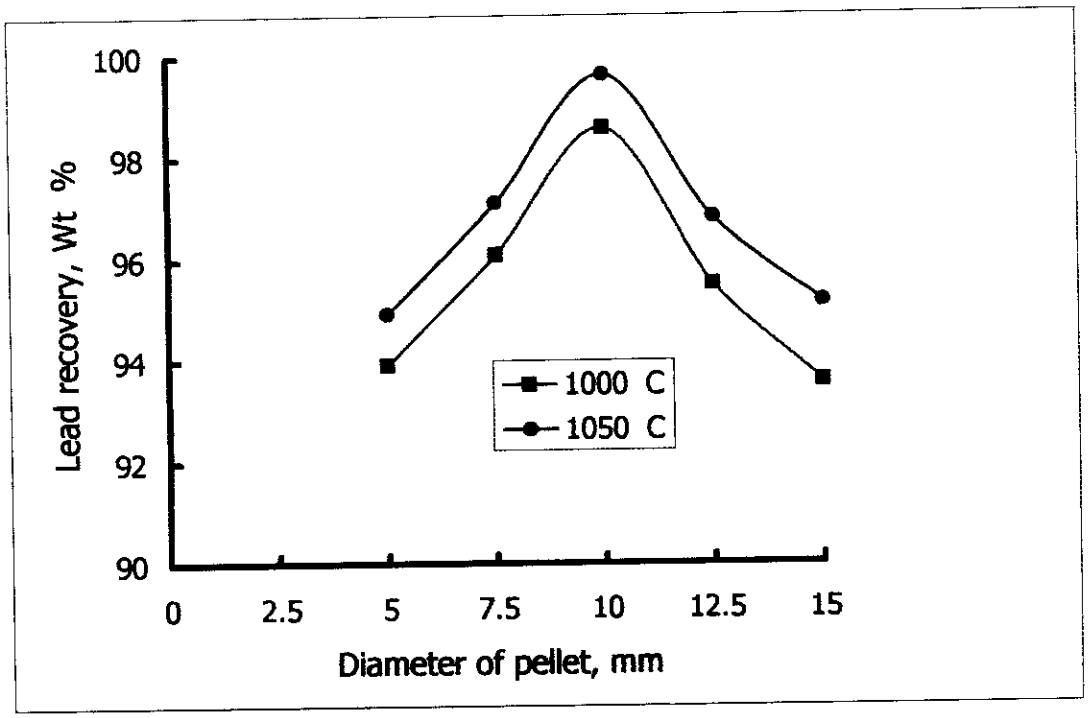

Fig.39 Effect of pellet diameter on the lead recovery by smelting at 1000°C & 1050°C.

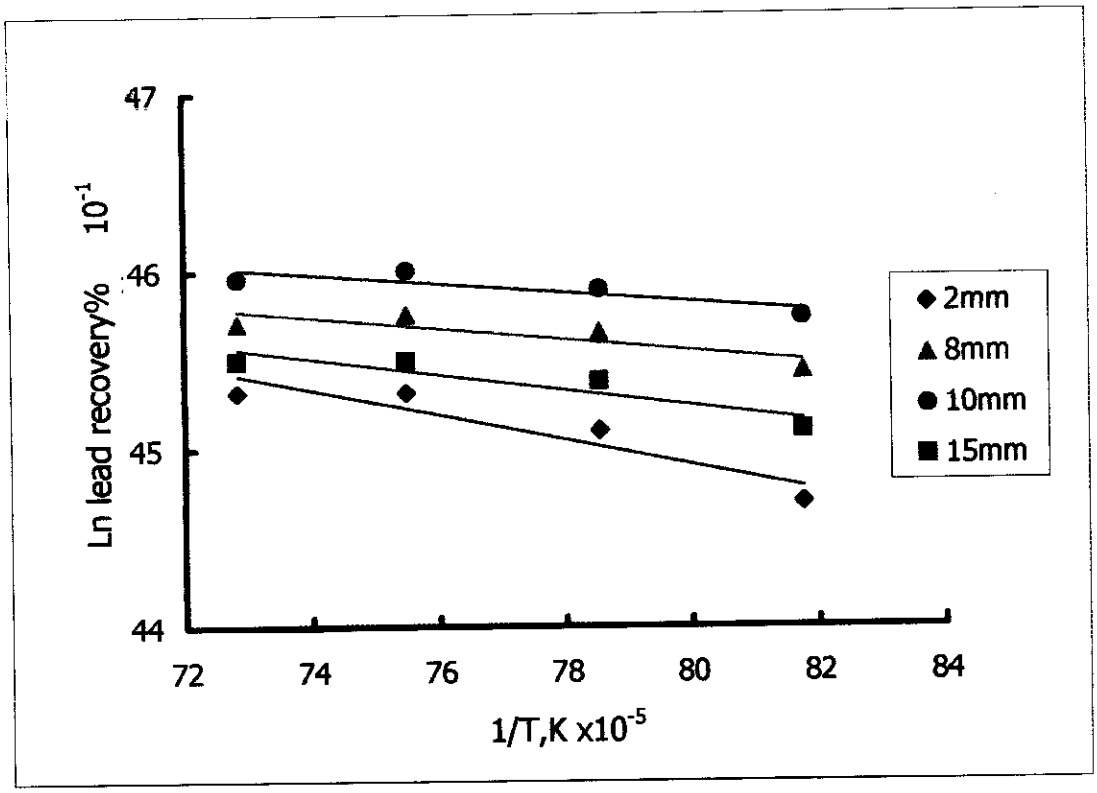

Fig. 40 The Arrhenius plot of the thermal recovery of metal lead from the prepared pellets.

3.9 Recovery of metal lead dust using hydrogen gas reduction.

Figure 41 shows the recovery percentage of metal lead (W_{mr}) as a function of the smelting temperature at constant time (15min.). It is seen that W_{mr} increases with increase in the temperature up to 1000°C. The maximum W_{mr} value (61.2) is achieved at 1000°C.

Figure 42 the Arrhenius plot of the thermal recovery of metal lead by hydrogen gas at constant time (15min.), the average ΔE value amounted to 7.789 KJ/ mol.

Figure 43 shows that the lead recovery increases with increases the time at constant temperature (1000°C). The maximum W_{mr} value (99.62) is achieved at 30 min.

Figure 44 shows the recovery percentage of metal lead (W_{mr}) as a function of the smelting temperature at constant time (30min.). It is seen that W_{mr} increases with increase in the temperature up to 1000°C. The maximum W_{mr} value (99.62) is achieved at 1000°C.

Figure 45 the Arrhenius plot of the thermal recovery of metal lead by hydrogen gas at constant time (30min.), the average ΔE value equal to 20.589 KJ/mol.

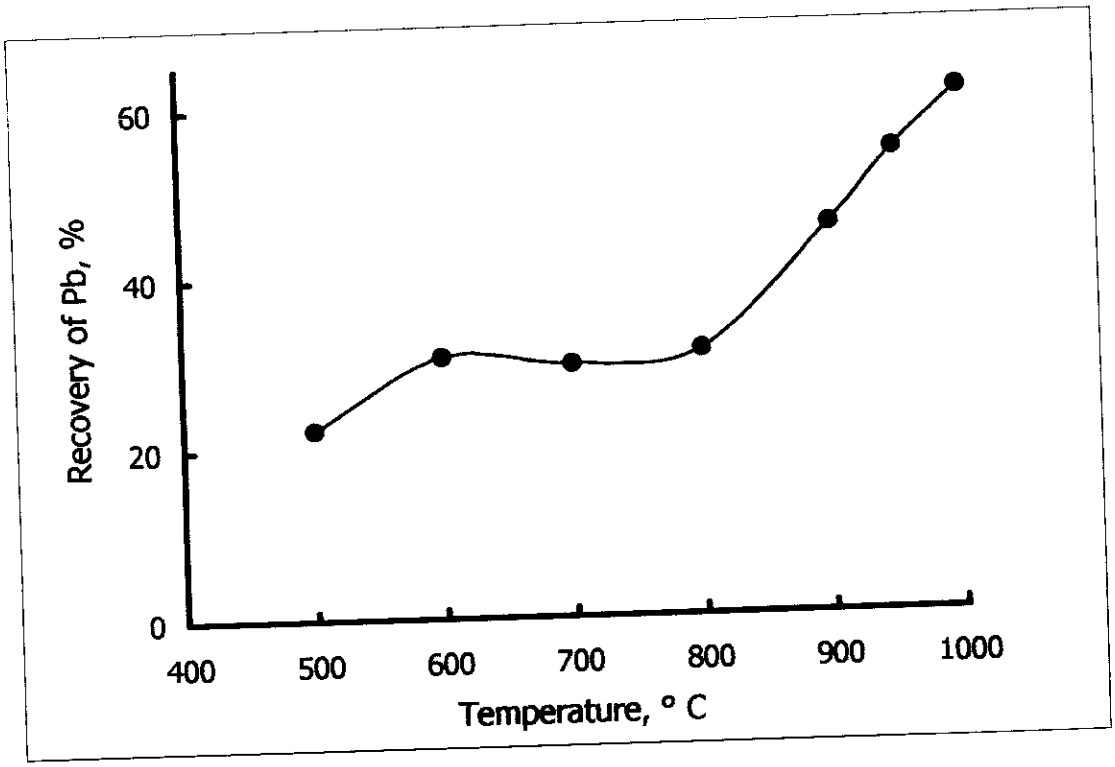

Fig. 41 The recovery percentage of metal lead as a function of the smelting temperature at constant time (15min.).

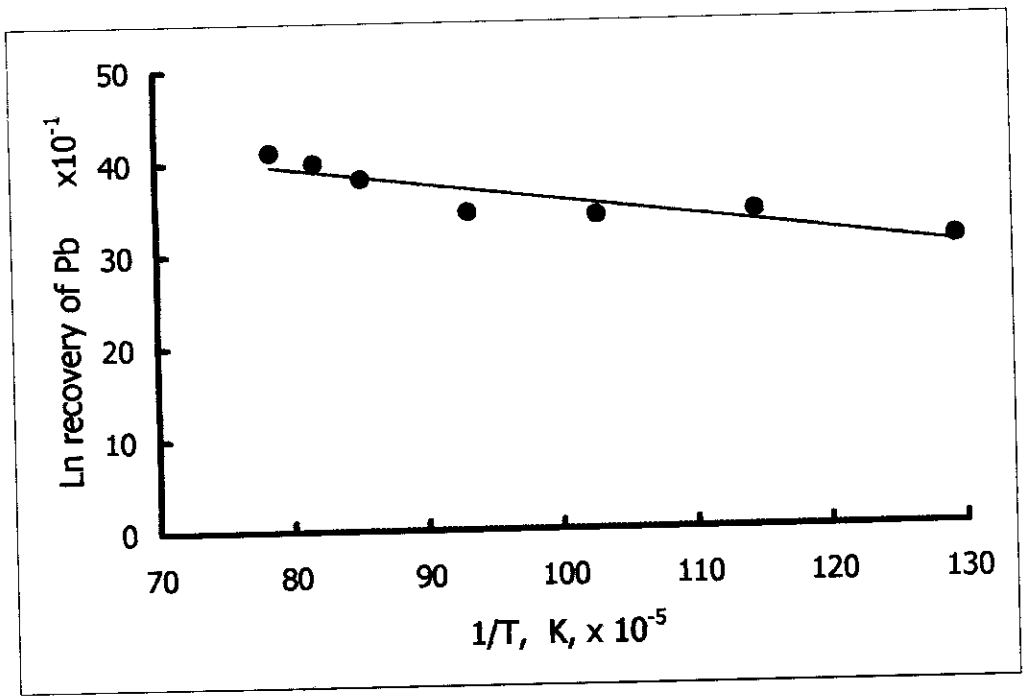

Fig. 42 The Arrhenius plot of the thermal recovery of metal lead by hydrogen gas at constant time (15min.).

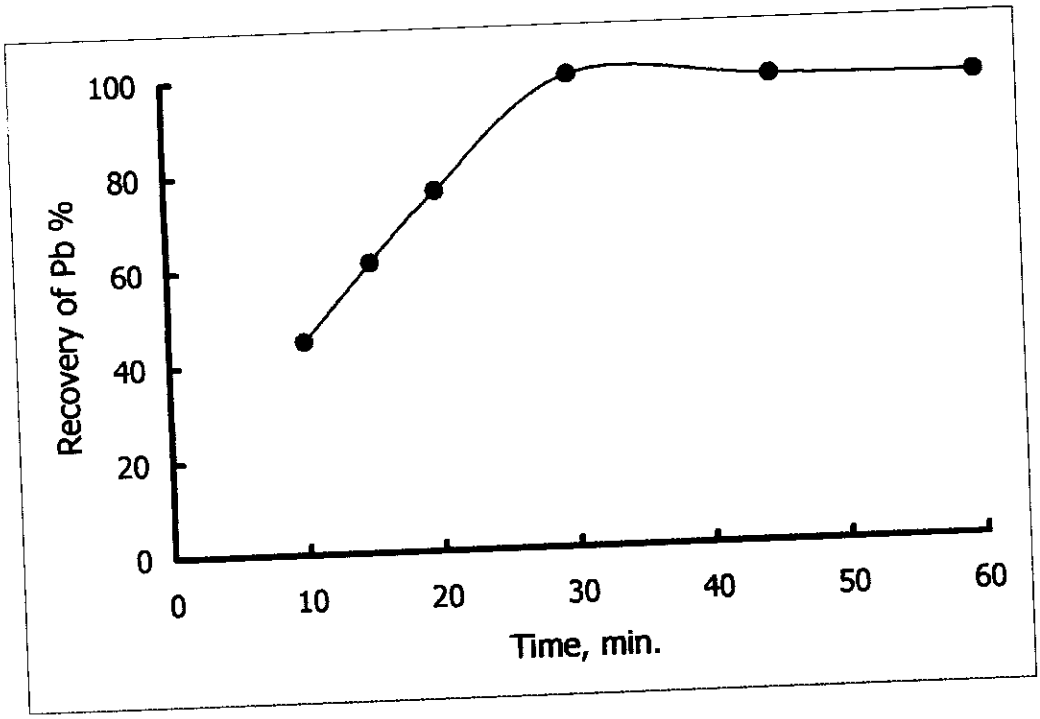

Fig. 43 The lead recovery as the function of time at the constant smelting temperature (1000 °C).

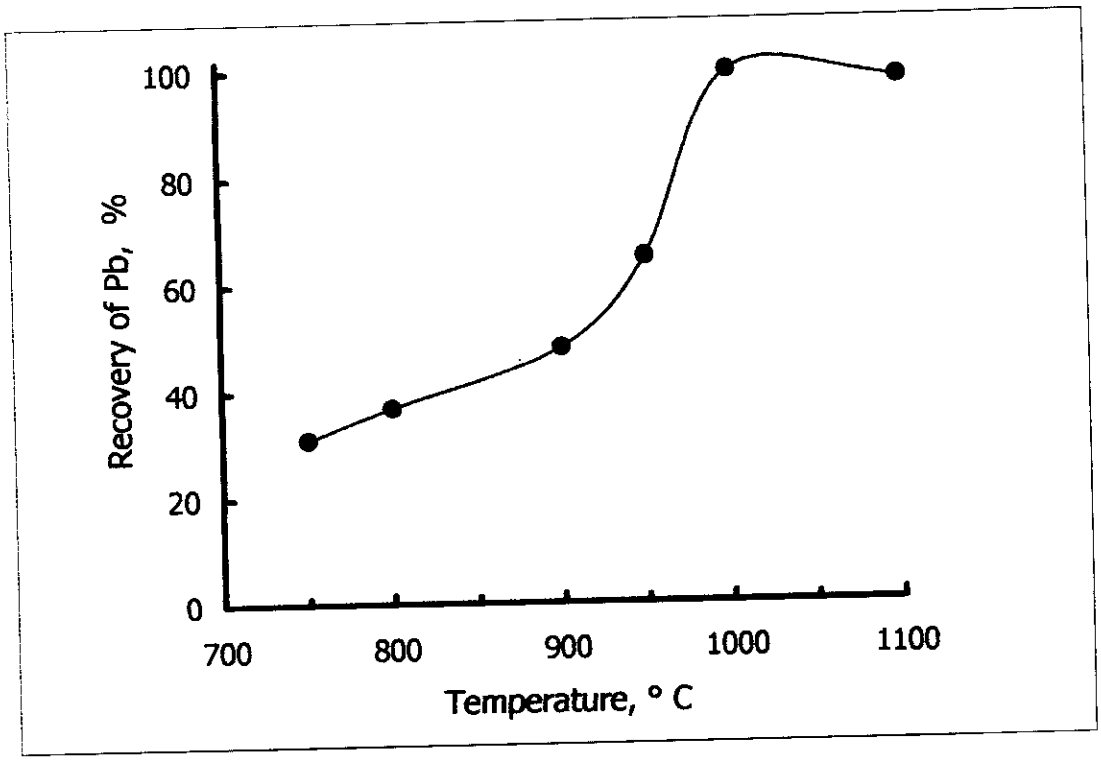

Fig. 44 The recovery percentage of metal lead by hydrogen gas reduction as a function of smelting temperature constant time (30min.).

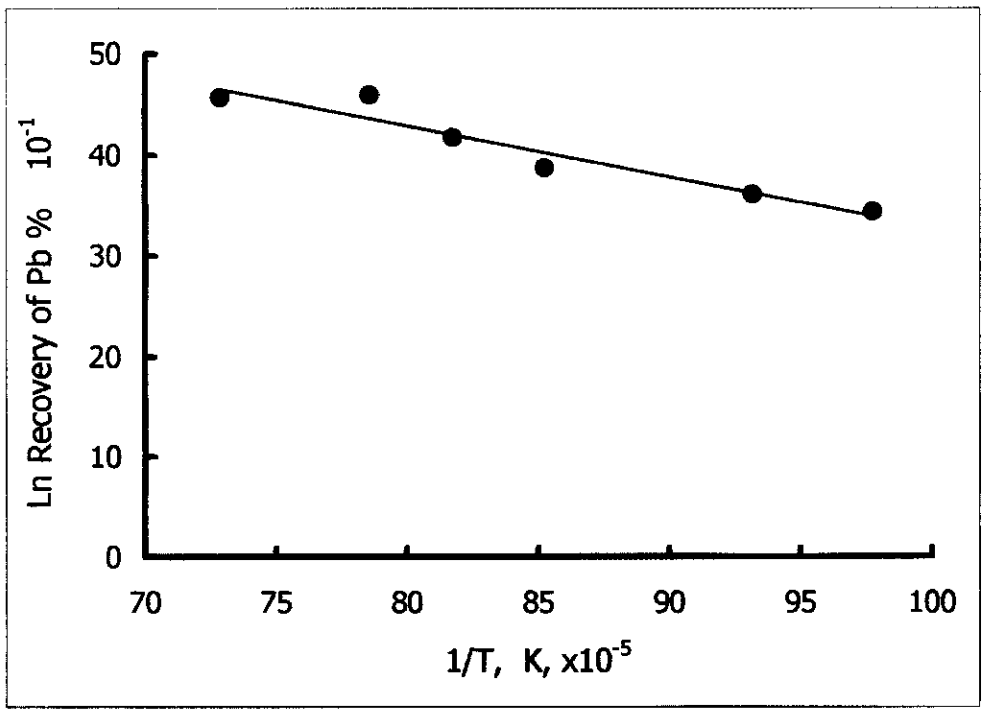

Fig. 45 The Arrhenius plot of the thermal recovery of metal lead by hydrogen gas at constant time (30min.).

3.10. Processing the results of the experiments

This part contains the calculation method of the slag samples of leaching process by using $FeCl_3$ solution, to find out the optimum conditions from our experimental results. So the chosen parameters that I used to carry on this calculation are L1, L2, L3 and L4; those I had described in the pervious chapter and the other parameters are:

$i = 1, 2,...N$ is the number of the trial.

b0 is the absolute values of mathematical model for the processing of the results of Pb

b1,..... are the coefficient values of mathematical model for the Processing of the results of Pb.

δ is the standard deviation or standard error for the processing result of Pb.

$y1_i$ is the yield in one trial for the processing result of Pb.

$y1_i = b0 + b1L1_i + b2L2_i + b3L3_i + b4L4_i$ is called the regression equation.

f is the number of degree of freedom.

k is the number of factors.

S1,.... are the variance of adequacy for the processing result of Pb.

F1,.. are Fisher ratio for the processing result of Pb.

$F1_t$, ... are Fisher ratio constant which is corresponding the degree of freedom.

3.10.1. Testing the adequacy of the model

If the Fisher ratio obtained for variances is greater than the value given in the table for the corresponding degrees of freedom and the selected significance level, this means that the significance of the variances differ from each other, i.e. that they are not homogeneous. The designing of experiment is called non-linear model. One of the frequently encountered kinds of non-linearity is connected with the fact that the effect of one factor depends on the level which another factor is at. In this case an interaction effect between four factors is said to take place. A factorial experiment makes it possible to quantitatively assess the interaction effects. For this purpose it is necessary to calculate the regression equation after adding the greater interaction effect and calculating the Fisher ratio. If the Fisher ratio obtained for variances is greater than the value given in the table, then an other interaction effect must be added to the regression equation, and so on, until the Fisher ratio obtained for variances is smaller than the value given in the table; this means that the significance of the variances are similar to each other, i.e. that they are homogeneous; and the designing of the experiment is called: the adequacy model.

3.10.2 Determination of the optimum conditions from experimental results.

i= 1...16

i	L1	L2	L3	L4	Z_L
1	-1	-1	-1	-1	85.5
2	1	-1	-1	-1	89.5
3	-1	1	-1	-1	87.0
4	1	1	-1	-1	92.0
5	-1	-1	1	-1	87.0
6	1	-1	1	-1	88.0
7	-1	1	1	-1	84.0
8	1	1	1	-1	87.0
9	-1	-1	-1	1	92.0
10	1	-1	-1	1	83.0
11	-1	1	-1	1	88.0
12	1	1	-1	1	87.0
13	-1	-1	1	1	91.0
14	1	-1	1	1	85.0
15	-1	1	1	1	87.5
16	1	1	1	1	88.0

$b0 = \Sigma Z_{Li} /16$ $\quad bo= 87.65$

$b1 = \Sigma L1_i Z_{Li} /16$ $\quad b1= -0.21875$

$b2 = \Sigma L2_i Z_{Li} /16$ $\quad b2= -0.09375$

$b3 = \Sigma L3_i Z_{Li} /16$ $\quad b3= -0.46875$

$b4 = \Sigma L4_i Z_{Li} /16$ $\quad b4= 0.03125$

$b12 = \Sigma L1_i L2_i Z_{Li} /16$ $\quad b12= 1.15625$

$b13 = \Sigma L1_i L3_i Z_{Li} /16$ $\quad b13= 0.031$

$b14 = \Sigma L1_i L4_i Z_{Li} /16$ $\quad b14= -1.71$

$b123 = \Sigma L1_i L2_i L3_i Z_{Li} /16$ $\quad b123= -0.075$

$b124 = \Sigma L1_i L2_i L4_i Z_{Li} /16$ $\quad b124= 0.65625$

$b134 = \Sigma L1_i L3_i L4_i Z_{Li} /16$ $\quad b134= 0.53125$

$b23 = \Sigma L2_i L3_i Z_{Li} /16$ $\quad b23= -0.46875$

$b24 = \Sigma L2_i L4_i Z_{Li} /16$ $\quad b24= 0.03125$

$b234 = \Sigma L2_i L3_i L4_i Z_{Li} /16$ $\quad b234= 0.406$

$b34 = \Sigma L3_i L4_i Z_{Li} /16$ $\quad b34= 0.65625$

$y1_i = b0 + b1L1_i + b2L2_i + b3L3_i + b4L4_i$

$\Delta y1_i = y1_i - Z_{Li}$

i	y1	Δy1	$(\Delta y1)^2$
1	88.40	1.90	3.61
2	87.9625	-1.5375	2.3639
3	88.2125	1.2125	1.4701
4	87.775	-4.225	17.8506
5	87.4625	0.4625	0.2139
6	87.028	-0.975	0.9506
7	87.275	3.275	10.7256
8	86.90	-0.10	0.010
9	88.4625	-3.5375	12.5139
10	88.025	5.025	25.2506
11	88.2125	0.2125	0.04515
12	87.8375	0.8375	0.7014
13	87.525	-3.475	12.0756
14	87.1763	2.1763	4.7365
15	87.3375	-0.1625	0.0264
16	86.90	-1.10	1.21

$f = N - (k+1)$ $\quad N = 16$ $\quad k = 4$

$f = 11$

$S1 = \{ \Sigma(\Delta y1)^2/f \}^{0.5}$ $\quad S1 = 2.919437$

$F1 = S1^2 / \delta^2$ $\quad \delta = 1.69$

$F1 = 2.984$ $\quad F1_t = 2.45$

$F1 > F_t$

$Y2_i = b0 + b1L1_i + b2L2_i + b3L3_i + b4L4_i + b12\ L1_i\ L2_i$

$\Delta y2_i = y2_i - Z_{Li}$

i	Y2	Δy2	$(\Delta y2)^2$
1	89.55	3.5625	9.3406
2	86.8062	-2.6935	7.2562
3	87.0562	0.05625	3.164×10^{-3}
4	88.9312	-3.06875	9.4172
5	88.618	1.61875	2.62035
6	85.868	-2.13125	4.54222
7	86.118	2.1187	4.48910
8	88.056	1.05625	1.11566
9	89.6187	-2.3812	5.6703
10	86.868	3.86875	14.967227
11	87.0562	-0.94375	0.89066
12	88.993	1.99375	3.97503
13	88.6812	-2.3187	5.3766016
14	86.0200	1.02005	1.040502
15	86.1812	-1.31875	1.7391016
16	87.0562	-0. 94375	0.890664

$f = N - (k+1)$ N= 16 k= 5

$f = 10$

$S2 = \{ \Sigma(\Delta y2)^2 / f \}^{0.5}$ S2 = 2.7080359

$F2 = S2^2 / \delta^2$ δ = 1.69

$F2 = 2.567$ $F2_t = 2.50$

$F2 > F2_t$

$Y3_i = b0 + b1L1_i + b2L2_i + b3L3_i + b4L4_i + b12\ L1_i\ L2_i + b34\ L3_i\ L4_i$

$\Delta y3_i = y3_i - Z_{Li}$

i	Y3	Δy3	$(\Delta y3)^2$
1	90.206	3.70625	13.736289
2	87.46245	-2.03755	4.15161
3	87.71245	0.71245	0.0507585
4	89.58745	-2.41255	5.82039
5	87.96175	0.96175	0.924963
6	85.868	-2.78825	7.7743
7	85.46175	1.4675	2.1367131
8	87.39975	0.39975	0.1598
9	88.96245	-3.03755	9.22671
10	86.21175	3.21175	10.315338
11	86.400	-1.60	2.560
12	88.336	1.336	1.78690
13	89.337	-1.6625	2.76407
14	86.676	1.67625	2.80981
15	86.8375	-0.6625	0.43890
16	87.7124	-0.2875	0.082685

$f = N - (k+1)$ $N = 16$ $k = 6$

$f = 9$

$S3 = \{ \Sigma(\Delta y3)^2/f \}^{0.5}$ $S3 = 2.6820$

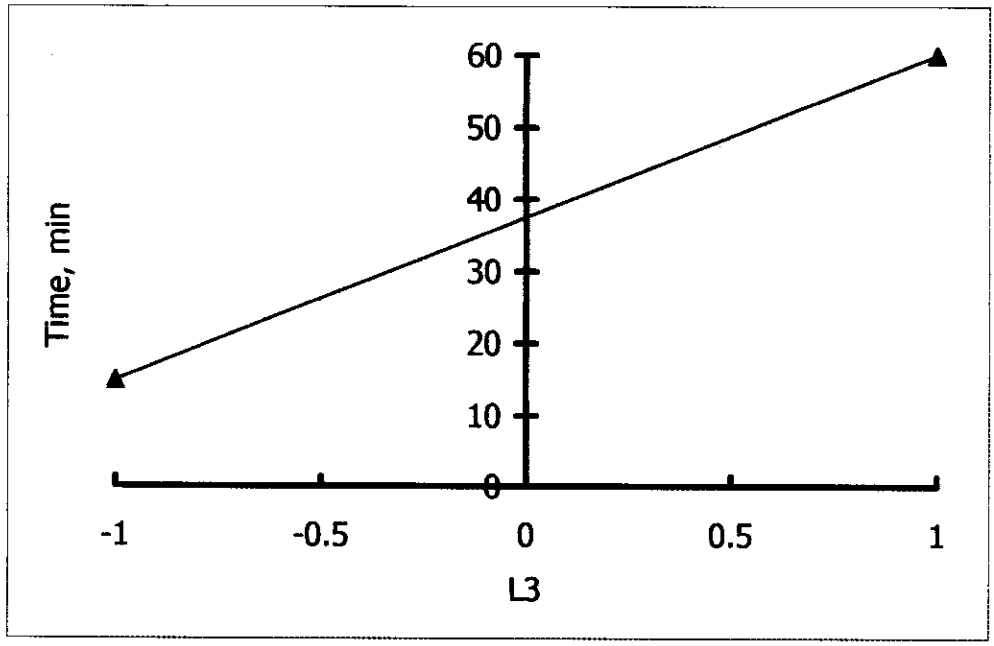

Fig.48 The standard diagram of time from experimental design.

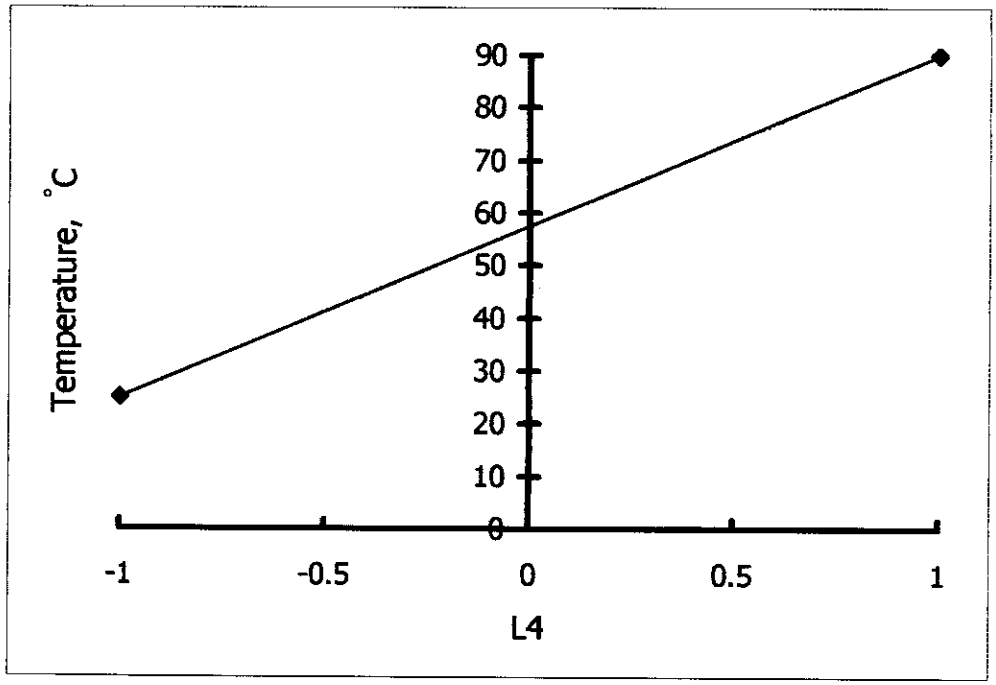

Fig.49 The standard diagram of temperature from experimental design.

3.11 Recovery of lead from slag.

Three ways applied to recover lead from slag:

1- The first way the ferric chloride leaching of slag. The recovery of lead from slag by ferric chloride leaching is 94%

2- The second way was to dissolve the slag in hot hydrochloric acid followed by filtration while hot. The filtrate was then cooled < 15 ° C. The precipitation lead chloride was obtained by filtration. Lead chloride was then carbonated wit sodium carbonate as with the dust sample. Lead carbonate so formed was the thermally reduced to metal lead at 1000 ° C. using hydrogen gas.

3- the third way was to dissolve the fine slag in 1M ammonium acetate followed by filtration. The dissolved lead compounds in the acetate solution were precipitated as lead chloride by acidification with hydrochloric acid to precipitate lead chloride. The lead recovery was the accomplished as shown above.

Figure 50 shows the solubility of lead chloride increase with increase the temperature the maximum value of lead chloride is 33.4 at 100° C. Figure 51 shows the leached weight obtained by acid leaching of the slag formed during the smelting process as a function of particle diameter of the slag. In some experiments, hydrogen peroxide is added to the leachant up to 25% by volume. Experiments were carried out at 75°C. It is seen that W_{ml} increases with the decreases in particle diameter of the slag and increases in percent volume of the H_2O_2 added. Complete leaching is acquired with particle diameter <0.63 mm and addition of 25% H_2O_2.

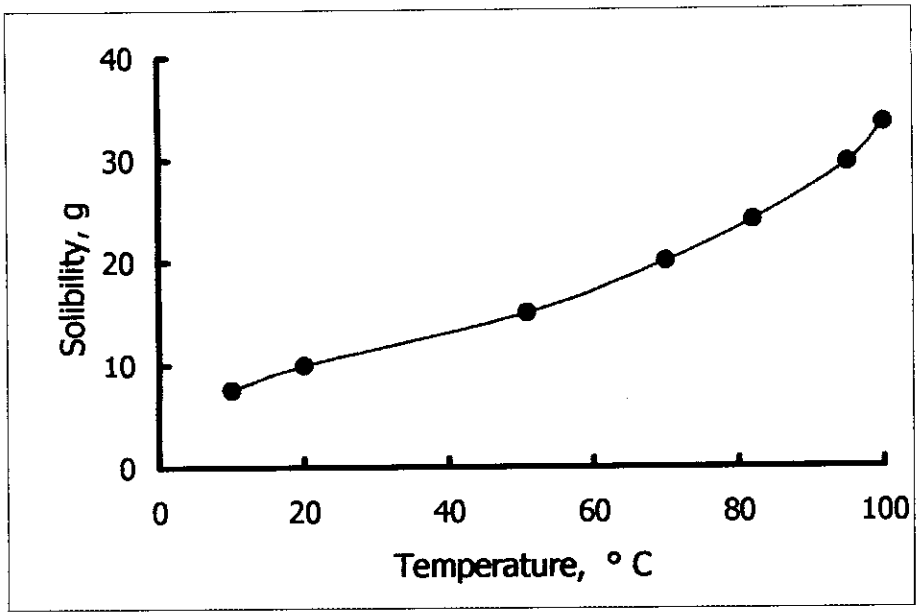

Fig 50. The solubility of lead chloride as the function of temperature.

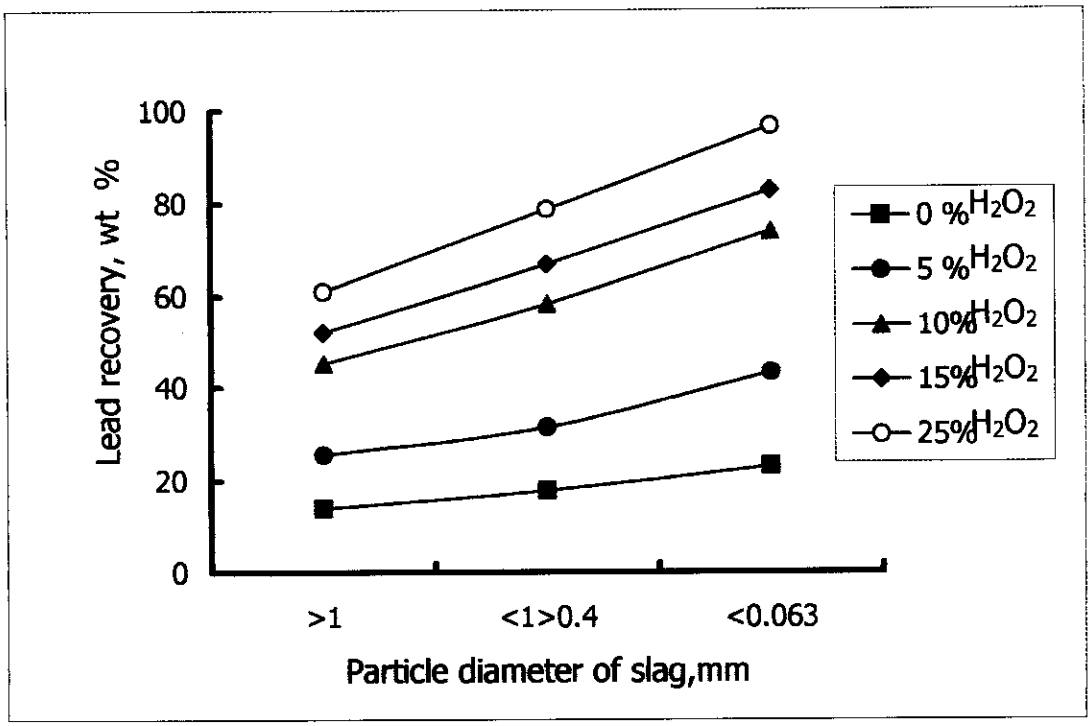

Fig. 51 Hydrometallurgical recovery % of metallic lead by leaching the slag having different particle diameter.